Chapter 15
Natural Gas Power

Raub W. Smith and S. Can Gülen

Glossary

Brayton cycle	The thermodynamic cycle describing the operation of a gas turbine. In a combined cycle, it is the *topping* cycle due to its relative position vis-à-vis Rankine cycle on a temperature–entropy surface.
Carnot cycle	Also known as the Carnot engine, it is the embodiment of the second law of thermodynamics in the form of a theoretical cycle comprising two isentropic and two isothermal processes. No heat engine operating in a thermodynamic cycle can be more efficient than the corresponding Carnot engine defined by the constant mean-effective heat addition and heat rejection temperatures.
Cogeneration	See combined heat and power (CHP).
Combined cycle power plant	A fossil-fired power plant that combines two types of prime movers, usually one or more gas turbines and one or more steam turbines (STs), whose operation are governed by their respective

This chapter was originally published as part of the Encyclopedia of Sustainability Science and Technology edited by Robert A. Meyers. DOI:10.1007/978-1-4419-0851-3

R.W. Smith (✉) • S.C. Gülen
GE Infrastructure-Energy, 1 River Road, Bldg 40, 4th Floor, Rm 412, Schenectady, NY 12345, USA
e-mail: raub.smith@ge.com; can.gulen@ge.com

R. Malhotra (ed.), *Fossil Energy: Selected Entries from the Encyclopedia of Sustainability Science and Technology*, DOI 10.1007/978-1-4614-5722-0_15,
© Springer Science+Business Media New York 2013

	thermodynamic cycles, i.e., Brayton and Rankine.
Combined heat and power (CHP)	The term used for fossil-fired power plants, which, in addition to their primary product, electric power delivered to the grid, also supply a secondary product in terms of useful thermal energy.
Combustor	A mechanical device to facilitate controlled mixing and reaction of an oxidizer (in almost all cases air) and a fuel (in almost all cases a pure hydrocarbon or a mixture thereof in gaseous or liquid phase) to generate high-temperature gaseous product for expansion in a turbine and useful shaft work generation.
Compressor	A mechanical device that increases the pressure of a gas by reducing its volume. There are different types of compressors, e.g., axial, radial, and reciprocating, which are suitable to different types of operating regimes.
Efficiency	Unless specified otherwise, the thermal efficiency of a power-generating system, which is the dimensionless ratio of generated kWh of electricity to the amount of energy required to generate it. It is the inverse of the heat rate with a suitable conversion factor.
Emissions	Gases and solid particles (usually undesirable) released into the air as by-products of a combustion process (e.g., in the boiler of a fossil-fired power plant, gas turbine combustor, or other internal combustion engine) to create electric power or propel a vehicle.
Firing temperature	The temperature of the gas turbine combustor exhaust gas at the inlet to the first stage rotor, which is the starting point of useful shaft work generation.
Gas turbine	A prime mover or internal combustion engine comprising a compressor, combustor, and an expander connected via

	a common shaft, through which air is compressed, burned, and expanded to generate useful shaft work for electric power generation (or thrust in an aircraft jet engine).
Generator	A device that converts the mechanical shaft power generated by a prime mover into electrical power.
Global warming	The apparent increase in the average temperature of the earth's near-surface air and oceans since the mid-twentieth century and its projected continuation (per *Wikipedia*).
Greenhouse effect	The containment of heat from solar radiation striking the earth's surface due to the earth's atmospheric "greenhouse" gases such as carbon dioxide and methane. These gases absorb and emit radiation within the thermal infrared range and are believed to be a primary cause of global warming.
Heat rate	Amount of energy required to generate 1 kWh of electricity. It is the inverse of the thermal efficiency with a suitable conversion factor.
Heating value	The thermal energy produced by completely burning a unit mass of fuel in a combustor to produce carbon dioxide and water. If the water is in a gaseous phase, the heating value is referred to as net or lower heating value (LHV). If the water is in a liquid phase, the heating value is referred to as gross or higher heating value (HHV).
Heat recovery steam generator (HRSG)	Also known as the heat recovery boiler (HRB), HRSG is a cross-flow tubular heat exchanger that recovers the exhaust heat from a prime mover (e.g., a gas turbine) and produces steam at high pressure and temperature that is used in a steam turbine (ST) for additional power generation. HRSG is the key equipment that "combines" gas and

	steam turbines in a combined cycle power plant.
Rankine cycle	The thermodynamic cycle describing the operation of a steam turbine. In a combined cycle, it is the *bottoming* cycle due to its relative position vis-à-vis Brayton cycle on a temperature-entropy surface.
Steam turbine	A prime mover or the power-generating part of an external combustion engine comprising one or more sections connected via a common shaft, through which steam flows, expands, and discharges to a condenser to generate useful shaft work for electric power generation or propulsion.

Defining the Subject

Natural gas is an important fossil fuel that has played an increasingly significant role in worldwide electric power generation since the 1980s. The key driver underlying the importance of natural gas as a vital enabler of modern living has been its relative advantage vis-à-vis other fossil fuels in terms of emissions and pollutants. In comparison to coal, the primary fossil fuel used for electric power generation in the world on a constant consumption basis, natural gas emits nearly 45% less CO_2, 80% less nitrogen oxides (NO_x) with negligible amounts of sulfur oxides, particulates, and mercury.

The environmental advantages of natural gas are further amplified by the significantly higher thermal efficiency of the power plants that burn it for electric power generation in comparison to other variants of oil or coal. Natural gas burning modern gas turbines can readily reach efficiencies of 56–57% in combined cycle configurations. This is well above the average efficiency of existing coal burning steam turbine plants (e.g., low 30s) as well as the most advanced ultra-supercritical designs thereof (e.g., low 40s).

With the beginning of the twenty-first century, economic projections pointed to natural gas as the fastest growing fuel for worldwide electric power generation, with an expected average annual rate of growth of about 3.7% between 2005 and 2030. During this period, natural gas will account for almost one-fourth of the world's total net electricity generation [1]. While such long-term forecasts are highly susceptible to uncertainties such as the impact of potential governmental policies or legislation

limiting the use of fossil fuels in favor of nuclear and renewable sources of energy (largely driven by concerns over global warming), it is almost a foregone conclusion that natural gas will continue to be an important part of the world's energy and electric power generation portfolio in the foreseeable future.

Given this impact of natural gas on future electrical production, it is important to establish a basic understanding of the history, current state of the art and future possibilities of power generation using natural gas combustion in order to have a complete picture of future energy sustainability.

Introduction

Natural gas is a fossil fuel comprising hydrocarbons, primarily methane (CH_4) up to 90% on a volumetric basis. It differs from the other fossil fuels in that it is naturally available as a gas (hence the name) as opposed to a solid (i.e., coal) or liquid (i.e., oil). Like other fossil fuels, the basic mechanism (thermogenic) of natural gas formation involves the extremely prolonged high-pressure compression of organic matter remains (e.g., plants, animals that lived millions of years ago on earth). The gaseous phase is the result of extremely high temperatures associated with the depth of the organic matter, typically 1–2 miles below the earth's crust. At even deeper levels, natural gas consists almost entirely of pure methane.

Another (biogenic) mechanism for forming natural gas is the chemical transformation of organic matter by microorganisms. The resulting gas contains methane and carbon dioxide. A well-known example of this mechanism is the landfill gas that results from the decomposition of waste materials deposited into large landfills. Other biogas formation mechanisms are sludge digestion in the tanks of sewage treatment plants (sewage gas) and anaerobic fermentation of agricultural waste. Biogas formation takes place near the earth's surface in the absence of oxygen and the resulting gas usually leaks to atmosphere. Controlled capture of landfill gas and other biogases for utilization in electric power generation is a promising technology. (Uncontrolled energy release (explosion) from the trapped landfill gas leading to death and destruction in the poverty-stricken areas of the world is an unfortunate event that appears in the news from time to time.) Biogas utilization is also important because the main constituent, methane, itself is a principal greenhouse gas (GHG). In fact, methane is nearly 20 times more effective than CO_2 in trapping heat emanating from the earth's surface. Therefore, combustion of methane (with resultant CO_2 emissions) that otherwise would leak into the atmosphere is a preferable trade-off from GHG reduction point of view.

Coal mine gas is another type of natural gas that is released during pit coal mining. Depending on the time of capture and method, there are different types. The most common types are coal bed methane (CBM) and coal mine methane (CMM). The former is largely pure methane and its production is independent of coal mining. The latter is released during active mining and presents a significant

Table 15.1 Composition and heating values of typical natural gases

Component (%)	Coal bed methane	Coal mine methane	Landfill gas	Biogas	Average NG
O_2	2.1	12.6	0–1	0–2	
N_2	8.2	46.8	2–5	0–10	1.6
CH_4	85.9	40.0	45–60	50–75	93.1
CO_2			40–65	25–50	1.0
C_nH_{2n}	3.8				4.3
LHV, kcal/nm^3	7,762	3,200	3,350–4,775	3,580–5,975	8,275
(Btu/scf)	872	360	375–535	400–670	930

danger of violent explosion to miners. Proper ventilation of mine shafts to remove and vent CMM into atmosphere is essential for the safety of mining operation. The methane content of CMM is variable (25–60%) and can change suddenly, which might be problematic for its use as a fuel. A third type of coal mine gas is abandoned mine methane (AMM), which can seep from mines that are no longer active. Annual coal mine methane emissions account for about 8% of total anthropogenic methane emissions or about 28 billion m^3 of carbon dioxide equivalent [3]. Utilization of CMM and AMM for power generation is critical to the prevention of release of a GHG into atmosphere.

Energy content of the natural gas is measured in terms of Btu (kJ or kcal) per lb (kg) or per standard cubic feet (cubic meters). In many practical calculations, natural gas is assumed to be 100% pure methane, which has an energy content of 21,515 Btu/lb (50,044 kJ/kg or 11,953 kcal/kg) on a lower heating value (LHV) basis or 914 Btu/ft^3 (34,050 kJ/m^3 or 8,133 kcal/m^3) at normal (standard) conditions (herein defined as 77°F (25°C) and 1 atm). The actual composition may vary depending on the source and treatment. Based on the mean of over 6,800 samples of pipeline quality natural gas taken in 26 major metropolitan areas of the USA [4], the methane content is 93.1% with a heating value of 930 Btu/ft^3 (8,275 kcal/m^3). A sampling of composition and heating value of most common natural gas variants is given in Table 15.1.

Production and distribution companies measure natural gas in volumetric terms, i.e., in multiples of cubic feet such as millions of cubic feet, trillions of cubic feet, etc. In power generation calculations, where natural gas is the fuel burned in the combustor of the gas turbine, the more practical approach is to use the mass flow rate (lb/s or kg/s) along with the LHV value or the product of the two, which is referred to as heat consumption (MMBtu/h or kW).

The purpose of a power plant is to generate electric power. Therefore, the key performance metric of an electric power generator is the net thermal efficiency, which is the ratio of the electric power measured at the generator terminals (after subtracting all the power that is spent to keep the plant running) to the plant's fuel energy consumption. The most efficient way to burn natural gas for electric power generation is in a gas turbine combined cycle (GTCC) power plant. Today's state-of-the-art CC power plant has a rated net efficiency of 58% on an LHV basis.

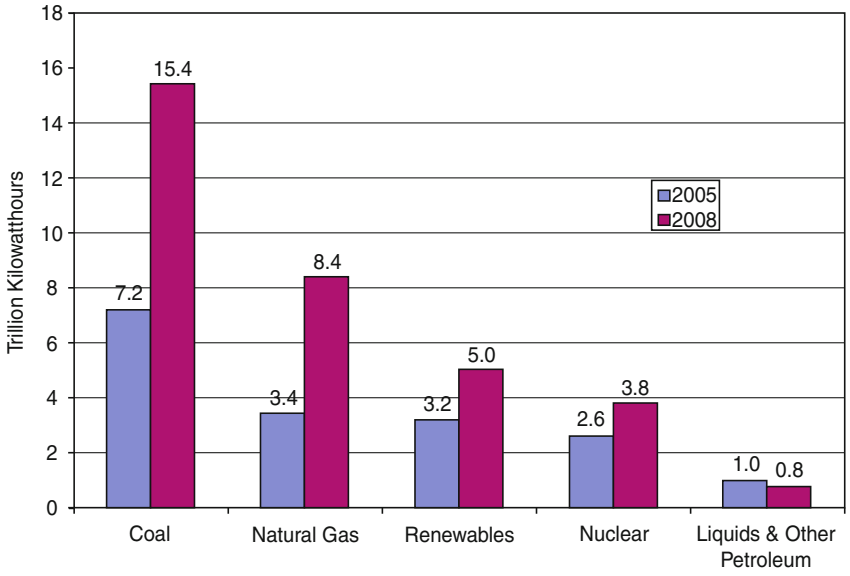

Fig. 15.1 World Net Electricity Generation. Renewables include hydroelectric (Source: Energy Information Administration (EIA) [1])

In other words, for each 1 lb/s of natural gas (about 23.5 ft^3/s as 100% methane) that enters the combustor of the gas turbine, (using the formula 58% × 21,515 Btu/lb × 1 lb/s × 1.05506 kWs/Btu = 13,166 kW) about 13.2 MW of electric power (net) is delivered to the grid. This is enough power to sustain nearly 13,000 average homes for 1 h at an average power consumption of 1 kW.

In 2005, natural gas accounted for 3.4 trillion kWh of net electricity production for about 20% of the world total (see Fig. 15.1). This contribution is projected to reach 8.4 trillion kWh in 2030 or about 25% of the world total corresponding to a total natural gas consumption of 55.5 trillion ft^3 (i.e., 35% of total world production of 158.6 trillion ft^3). Using the calculation above as a rough guide, this translates into an average natural gas–fired power plant thermal efficiency of 56.4%. The natural gas reserves of the world are estimated at about 6,186 trillion ft^3 with top 20 countries contributing nearly 90% of it (see Fig. 15.2). When one considers the uncertainty in the cited projections, it appears safe to say that there are ample deposits of natural gas to sustain electric power production well into the twenty-first century.

As mentioned in the beginning, natural gas is a superior fossil fuel in terms of emissions and pollutants vis-à-vis other fossil fuels, i.e., coal and oil. This is not to say that natural gas is totally harmless, especially when one considers the emissions of CO_2 – the most abundant anthropogenic greenhouse gas in the atmosphere and, as such, the main culprit suspected in driving global warming. A modern gas turbine combustor generates 2.75 lbs of CO_2 per lb of natural gas burned. In other useful relative terms, this is approximately 129,000 lb (58,500 kg) of CO_2

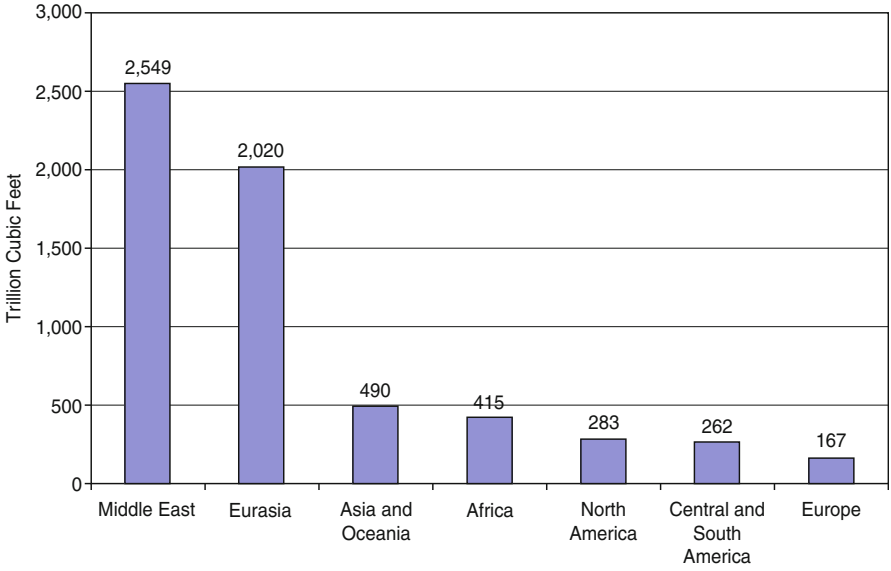

Fig. 15.2 World Natural Gas Reserves, January 2008. Asia, Oceania and Europe exclude countries that were part of the former USSR whereas Eurasia includes only those. Source: Energy Information Administration (EIA) [2]

per billion Btu (1.06 million MJ) of energy input or 1,125 lb/MWh generated by a gas turbine (GT) in simple cycle configuration (cf., 750 lb in combined cycle configuration). Since not all power generation equipment performs at today's higher efficiency level, real averages would be higher, e.g., 1,300 and 800 for simple and combined cycles, respectively. For the projected natural gas–based electric power generation in 2030 cited above, at a rate of 1,300 lb/MWh, this translates into 5 billion metric tons of CO_2 released into earth's atmosphere. (In order to get an idea about the magnitude of this number, consider that the estimated weight of carbon dioxide in the atmosphere was about 2,163 billion metric tons before the industrial revolution.) This is approximately half of the total 2030 projection of CO_2 emission from natural gas combustion, which itself is about 20% of the 42.3 billion metric tons for all fossil fuels.

While an important contributor to the greenhouse effect, natural gas is extremely advantageous from the perspective of two other significant combustion-related pollution phenomena, i.e., smog and acid rain. Smog (whose primary constituent is ozone) is formed by a chemical reaction of carbon monoxide, nitrogen oxides, volatile organic compounds, and heat from sunlight [5]. Acid rain is formed when sulfur dioxide and nitrogen oxides react with water vapor and other chemicals in the presence of sunlight to form various acidic compounds in the air [5]. Natural gas combustion products are virtually free of the two main culprits contributing to these severe pollution problems, namely, sulfur oxides (SO_x) and particulate matter, and they have 80% less NO_x than products of coal combustion.

In general (notwithstanding some future fuel cell designs discussed later), the most efficient means to utilize natural gas as a fossil fuel in electric power generation is to burn it in internal combustion (IC) engines. The two most widely used IC engines in electric power generation are gas turbine and reciprocating internal combustion or diesel engine. (Note that the term *diesel* in this context refers to the thermodynamic cycle of the compression-ignition (CI) IC engine and not the fuel.) While possible in theory, natural gas is not used with external combustion technology (e.g., boiler and steam turbine plants) due to the pronounced superiority of the IC engines in efficiency, emissions, power density (i.e., favorable cost vs. size trade-off) and operational flexibility.

Modern gas turbines are large air-breathing turbomachines with extremely large power output. For example, consider a 50-Hz (3,000 rpm) 300+ MW net power output unit as listed in a 2008 trade publication [6]. This machine ingests air at ISO conditions (15°C and 1 atm at 60% relative humidity) at a rate of nearly 1,550 lb/s (705 kg/s), compresses it to a pressure that is 18 times that of the ambient and combusts it with about 35 lb/s (16 kg/s) of natural gas (100% CH_4) generating 312 MW net electric power for a net thermal efficiency of 39.3%. At the inlet to the expander section of the gas turbine, where they produce useful shaft work, the combustion products are at nearly 1,500°C (2,732°F). This is well above the melting point of the most advanced superalloy materials that are used in the manufacture of turbine expander components. In order to ensure the survival of the turbine parts under those extreme conditions for thousands of hours of continuous operation, nickel-based superalloy components are protected by thermal barrier coatings (TBC) and internally cooled by using the "cold" air extracted from the turbine compressor. (Consider that without cooling and TBC, the first stage vanes of a modern GT would survive barely ten seconds before melting away.) Utilizing those and other technologies, some of which are adopted from the advanced military and civilian aircraft engine–related research and development, land-based heavy-duty industrial gas turbines are true marvels of human engineering.

Diesel or compression-ignition IC engines are no slouches themselves. In fact, the efficiency of a tri-fuel (one that can burn natural gas, light and heavy fuel oils) unit rated at nearly 17 MW net electric output is 47.3% on an LHV basis when operating with natural gas fuel [7]. They are eminently suitable to landfill, biogas, and coal mine gas applications. They are at a disadvantage because of their relatively low power density and cost. The sample multifuel diesel engine cited above has a power density of 0.05 kW/kg of engine weight or 215 kW/m^2 of engine footprint. These numbers compare very unfavorably to the power density of a heavy-duty industrial gas turbine. For a typical advanced machine with the performance similar to the sample cited above, the power density is about 0.8 kW/kg of engine weight or about 3,000 kW or more per m^2 of engine footprint. In order to appreciate the power density of a GT vis-à-vis renewable energy–based systems, consider that the power density of typical wind and solar radiation are 0.4–0.8 (depending on altitude and speed) and 1.4 kW/m^2, respectively [8]. One would need hundreds of acres of wind turbine farms or solar collector fields to replace a single advanced F-Class gas turbine. This gross disparity in the power density of the two IC engine technologies is reflected in the annual unit

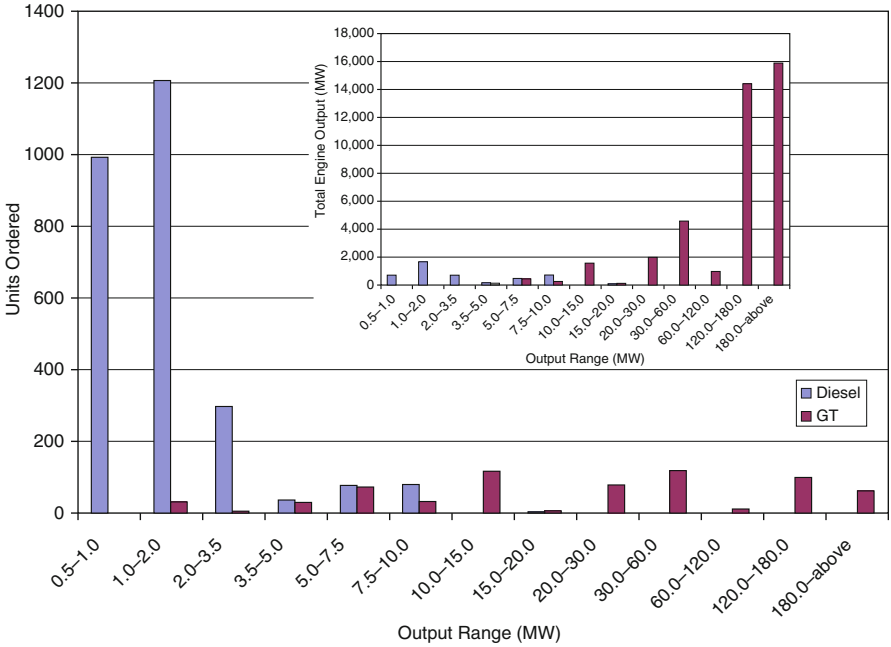

Fig. 15.3 Dual-fuel and natural gas diesel engine and gas turbine orders, June 2005 through May 2006 [9]

order numbers displayed in Fig. 15.3. In terms of the numbers of units ordered in 2005–2006 [9], reciprocating IC engines dominate (nearly 2,700 units vs. 666 for gas turbines) but the significant bulk of the orders are for units rated at 3.5 MW or less. In terms of the total MW rating of the orders, all dual-fuel and natural gas diesel engines add up to 4.4 GW as opposed to more than 40 GW for all gas turbines.

At this point, it should be fairly obvious that a treatise on the subject of electric power generation using natural gas is essentially a treatise on modern land-based or heavy-duty industrial gas turbines. This is especially true for the past and the present of the technology. The future of electric power generation using natural gas as a fuel source might have a place for the fuel cell technology (with or without gas turbines). Ongoing research activities include solid oxide (SOFC), molten carbonate (MCFC), and polymer electrolyte (PEFC) technologies. From where one stands today, the most promising use for these technologies seems to be found in the fields of transportation and portable power. With the exception of distributed power generation, in which small-scale (1–500 kW) units power individual residences, office buildings, etc., the prospect of fuel cell–based technologies to replace internal combustion engines and specifically gas turbines as large-scale base load power-generating units in the near term, especially in a cost-effective manner, is practically nil.

A Brief History of Natural Gas

Natural gas has been around for quite a while. In China, nearly 2,500 years ago, early innovators used natural gas escaping naturally from the ground to light their temples and heat brine for distillation. Bamboo sections, split lengthwise, were glued together, and bound with twine, allowing the gas to be transported. In the early seventeenth century, French explorers near Lake Erie reported seeing natives burning gas naturally seeping from the ground. The first industrial use of natural gas can be traced back to England in the late eighteenth century when gas produced from coal was used to light houses and streets. In the USA, the first natural gas well was dug in 1821 in Fredonia, NY, four decades before Colonel Drake hit upon oil and gas at a depth of 69 feet in Lake Erie, PA. The well, dug by William Hart, was 27 ft deep in a creek bed. The extracted gas was transported through hollow log pipes to Fredonia for use in street lamps. Throughout most of the nineteenth century, natural gas was used almost exclusively for the same purpose, i.e., lighting. Following the invention of the Bunsen burner in 1885, natural gas also presented households with a more convenient means of cooking and heating. The main impediment to a wider utilization of natural gas was the lack of a transportation mechanism. The primary method, still in use today, is through an underground pipeline. While the first significantly long pipeline was constructed in 1891 (120 miles long between central Indiana and Chicago), it was only after World War II when technology advances made construction of longer and more reliable pipelines feasible. Until that time, natural gas was either allowed to vent into the atmosphere (intentionally or unintentionally) or burned in flares (as a by-product of coal mining and oil exploration) or just left in the ground when found alone. In fact, when the first astronauts looked at earth from the orbit, the most prominent sights on the earth's surface were the flares from the oil fields in Middle East and Africa. Even now about 150 million m^3 of natural gas, roughly equivalent to annual US residential consumption, is flared to the atmosphere. The contribution of the flared natural gas (NG) to global GHG emissions is about 400 million metric tons, equivalent to nearly one third of the annual US car exhaust emissions.

Today natural gas is used for much more than street lighting or household cooking. In fact, residential use of natural gas accounts for only a fifth of the total US consumption, with more than 60% used by the industrial sector including electric power generation. Until the end of 1980s, high-efficiency fossil fuel (mainly coal) firing or nuclear-powered steam turbine–based power plants supplied the base load electric generation capacity (6,000–8,000 h/year). When newly designed high-efficiency steam plants entered the service, older less-efficient units were relegated to intermediate duty operation (e.g., 4,000 h/year). Early generation, low-efficiency gas turbines, along with old steam plants and hydro pumped-storage plants, were largely limited to short-duration, peak-shaving-type operations. Due to changing economic parameters, introduction of protective environmental regulations, and major technological advances in gas turbine technology, starting in mid-1980s and early 1990s, natural gas became the fuel of choice for

new power plants. The steady increase in coal-fired steam plant efficiencies leveled off at the low 40% range, whereas new "F-Class" gas turbines with high firing temperatures, almost exclusively in combined cycle configuration, opened the door for thermal efficiencies easily exceeding 50% and even pushing for 60%. Recently, especially during the so-called energy boom of early 2000s, a large fraction of new capacity addition in the USA has been in natural gas–fired units, e.g., nearly 95% or 22 GW in 2000. Since then, this rate has tapered off significantly. Natural gas–fired power plant capacity addition in terms of construction starts totaled about the same, i.e., 22 GW, in the years 2005–2007 [10]. Scheduled construction start is about 9 GW for 2010, about the same as in 2009 but lower than the peak year of 2008 with nearly 12 GW. As pointed out earlier, natural gas is projected to be the fastest growing fuel for worldwide electric power generation. Thus, the pace of construction and commissioning of plants burning natural gas might be expected to pick up again. Construction of natural gas–fired power plants scheduled to start between 2011 and 2015 was estimated to be 44.5 GW [10]. Even though some projects will undoubtedly be cancelled or postponed, this is a strong positive sign for the future role of natural gas in electric power production.

The driver of the ascendancy of natural gas as the star of fossil fuels is the gas turbine, which also plays a key role in its transportation and distribution via huge pipeline networks. Heavy-duty industrial and/or aeroderivative gas turbines drive the large centrifugal gas compressors, which increase the pressure of natural gas up to 1,500 psia (∼100 bar). In most cases, these gas turbines burn the natural gas taken from the pipeline. Additional compressor stations, placed at regular intervals along the hundreds of miles long pipelines, maintain line pressures reduced via friction between pipe and gas, which can reach flow velocities up to 40 km/h.

A Brief History of Gas Turbine

When lieutenant colonel Heinz Bär died in a civilian aircraft accident in 1956 in (then) West Germany, he was the world's leading jet fighter ace with 16 victories to his credit. Some five decades after his death and more than six decades after his last aerial exploits, he is still unrivaled. The machine that enabled Bär to permanently enter the annals of military history was the world's first mass production jet fighter, the Messerschmitt Me-262. It was powered, remarked another famous German fighter pilot, "as if pushed by angels" – actually two 1984-lb thrust Jumo-004 gas turbine jet engines.

Developed under the leadership of Franz Anselm, the Jumo-004 was essentially the engine that opened up the jet age. Quite naturally, Dr. Anselm did not conceive Jumo-004 in a vacuum. Paraphrasing Sir Isaac Newton, he was standing on the shoulders of giants such as Sir Frank Whittle and Hans von Ohain, who are widely recognized as the pioneers of modern turbojet engine. Sir Frank and Dr. Ohain themselves almost certainly acknowledged early inventors such as Barber (first GT

patent in 1791), Stolze (first GT to be built and tried in 1900–1904), Holzwarth, and others, who showed them the path to the ultimate gas turbine engine design through their patents on air and steam turbines.

It is futile to attempt to plot a straight historical line from Hero's turbine (which had no purpose other than entropy generation) to today's modern 2,600°F firing temperature class steam-cooled H-System™. Countless inventors laid down the building blocks that eventually led to the modern gas turbine engine. For an excellent short history of turbomachinery in general and gas turbines in particular, the reader should consult the relevant chapter in Wilson and Korakianitis [11], who highlight the contributions of lesser known (unfairly) inventors such Aegidius Elling and George Jendrassik. Another good narrative with an emphasis on turbojets and German research and development can be found in Hans von Ohain's foreword to Mattingly's book on gas turbine propulsion [12]. For a detailed look at turbojet development activities of Sir Frank Whittle and Hans von Ohain in their respective countries, three articles by Meher-Homji can be consulted [13–15].

Quite obviously, wars or the prewar atmosphere of the western world in the first half of the last century pushed the development of gas turbines primarily as a military aircraft propulsion device. Starting in the late 1940s and early 1950s, engineers in USA and UK managed to derive robust, land-based power generation and, later, marine propulsion engines from these aircraft designs. Claire Soares essentially came to the conclusion that the involvement of so many people from so many different countries with immense pride in their work led to selective "histories" favoring selected milestones [16]. Her brief summary can be consulted for alternate takes on the development history of gas turbines. For a history of Siemens gas turbine development, a good resource is the paper by Leiste [17]. For a US perspective with an emphasis on GE, the reader should consult Miller and Nemec [18] and Brandt [19]. The paper describing the design and development of the GE MS7001F gas turbine by Brandt [20] is a good reference laying out all design aspects of a modern gas turbine and the trade-offs that are unavoidable in bringing a feasible product into the market.

Even though the development of the modern gas turbine was primarily driven by military and, to a lesser extent, civilian aircraft propulsion considerations, the introduction of stationary (land-based) units dedicated to power production did not lag too far behind. In fact, Aurel Stodola credited Hans Holzwarth with "having built the first economically practical gas turbine [21]." Holzwarth built several types of his "explosion" turbine in the first quarter of the twentieth century. Holzwarth's turbine was, strictly speaking, a hybrid construction combining the spark-ignition (constant volume) combustion process of an Otto cycle with the axial expansion process of a Brayton cycle. Stodola calculated a thermal efficiency of 25.6% for the test of a 1,500-rpm experimental turbine in Mühlheim–Ruhr in 1919 [21]. Burning a gas with 434 Btu/ft^3 heating value the turbine produced about 725 kW. Air and fuel gas was compressed by steam turbine–driven compressors and sequentially injected into the explosion chamber (gas first) at about 30 psia. Stodola reports an average maximum explosion pressure of 160 psia. The combustion products expanded through a two-stage velocity-compounded turbine. Exhaust gas at about 800°F was recovered in an exhaust heat boiler. In that sense, this unit

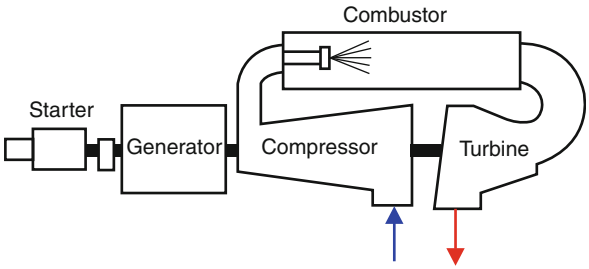

Fig. 15.4 Schematic diagram of Brown Boveri Co.'s Neuchâtel gas turbine (1939)

could be considered the first combined cycle. Holzwarth designed and developed several different variants of his turbine between 1907 and 1928. From 1928 on, Brown Boveri Company (BBC) took over the development of Holzwarth turbine and in 1933 installed a blast-furnace gas (BFG)–fired unit in a German steel mill, which was destroyed during World War II.

It is generally accepted that the first commercial stationary gas turbine for electric power generation was erected in Neuchâtel, Switzerland, by the former BBC in 1939, 3 years before the first flight of Me-262 powered by Jumo-004. This fuel oil burning 4 MW machine, primarily used for stand-by and peaking duties, was operational for nearly 70 years (see Fig. 15.4). The combustion chamber was derived from the turbocharged *Velox* boiler, which itself resulted from the BBC work done on the Holzwarth turbine. The BBC turbine was tested under the supervision of Aurel Stodola, who reported an overall thermal efficiency of 17.4%, which is less than half of the efficiency of today's advanced F-Class machines [22]. This machine was designated by the ASME as a *Historic Mechanical Engineering Landmark* in 1988.

The first gas turbine installed in an electric utility in the USA (Oklahoma Gas & Electric, Belle Isle Station, Oklahoma) was a 3.5 MW GE Frame 3 unit that entered service in 1949. In addition to generating power, the exhaust gas of this gas turbine was utilized to heat the feed water of a conventional steam plant. In other words, the first US electric utility gas turbine was in a "combined" cycle configuration [23]. In fact the combined cycle concept goes back to Emmet's mercury-vapor process (1925) [24]. For a brief history of the CC power plants and pertinent references, the reader should consult the 1994 Calvin Winsor Rice Lecture by Sir John Horlock [24].

One can look at the technology history of the land-based gas turbine and combined cycle power plants for electric power production in four generations:

1. Generation 1 (1949–1968)
   (a) Smaller than 30 MW GTs (Frames 3 and 5)
   (b) Firing temperatures 1,500–1,800°F
   (c) For repowering and cogeneration
2. Generation 2 (1968–1990)
   (a) B and E Technology GTs (50–120 MW)

(b) Firing temperatures ~2,000°F
(c) NO_x emission control using GT water/steam injection or SCRs
(d) Non-reheat steam cycles

3. Generation 3 (1990–1998)

(a) F Technology GTs (75–260 MW)
(b) Three air-cooled turbine stages
(c) Firing temperatures ~2,400°F
(d) Performance fuel heating (365°F)
(e) DLN combustion system for NO_x control
(f) Three-pressure, reheat (3PRH) steam cycles

4. Generation 4 (1998–present)

(a) H technology GTs (400+ MW in CC)
(b) Closed-loop steam cooling (CL-SC) of the first two turbine stages (both stator and rotor); four turbine stages
(c) Cooling of cooling air (CAC) for turbine wheel spaces and subsequent stages via a heat exchanger (a kettle reboiler) that generates IP steam to be used in the bottoming cycle
(d) Active clearance control (compressor and turbine)
(e) Firing temperatures ~2,600°F
(f) Performance fuel heating (400+°F)
(g) DLN combustion system for NO_x control
(h) Three-pressure, reheat (3PRH) steam cycle integrated with the GT Brayton cycle

The historical advances in GT firing temperature and CC efficiency is summarized in Fig. 15.5. The data illustrates the significant advance in the thermal efficiency of the GT combined cycle power plants, to the tune of nearly 15 percentage points, which is mainly driven by advances in materials, coatings, and cooling techniques that pushed the firing temperatures by almost 800°F (~450°C). In the following chapters, the reader is introduced to the basic thermodynamic principles that govern the performance of natural gas–burning gas turbine power plants. In addition, also provided is a brief overview of state-of-the-art gas turbine power plants, key economic criteria, and operability considerations. Finally, the future directions in gas turbine–based electric power generation systems are briefly elaborated upon.

Gas Turbine Power Plants

Gas turbine in itself or as a key component of a larger power generation system is a subject that can only be covered in dedicated books. Such books do exist and several selected treatises on the subject, which in the opinion of the authors reflect

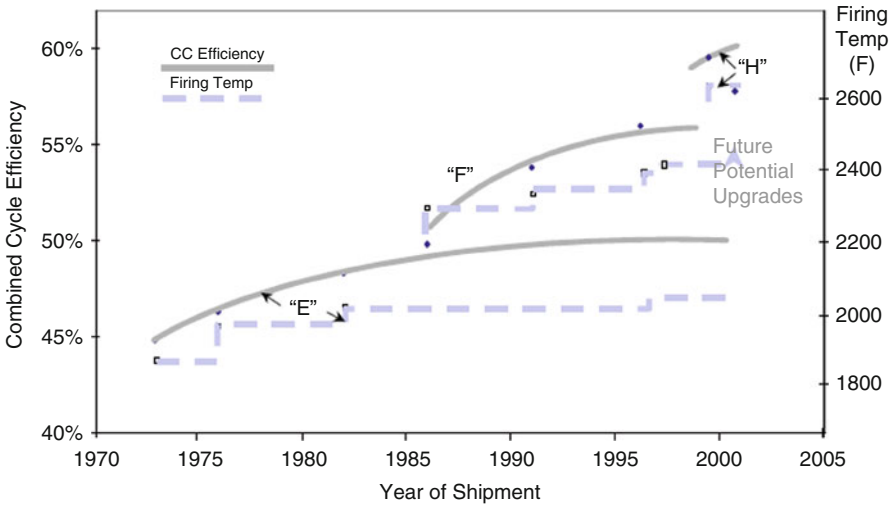

Fig. 15.5 Incremental evolutions of E-, F- and H-Class GT technology (From Ref. [25])

the best available published work in the field, are listed among the bibliography references. The coverage of the subject in the limited space allotted to the current chapter aims to provide the reader with the fundamental thermodynamic considerations that lead from the Carnot cycle to the present-day advanced gas turbine in a logically coherent manner. There is a reason that the gas turbine combined cycle plant is the most efficient heat engine that is commercially available today and, most likely, in the foreseeable future. That reason is embedded in the laws of thermodynamics. Understanding this will enable someone with a basic knowledge of key engineering concepts to grasp the gas turbine design principles and carry out nearly all calculations using simple formulas and a few technology charts. Furthermore, this will also enable the reader to critically evaluate new developments and claims to future improvements in electric power generation systems that employ turbomachines and utilize fossil fuels such as natural gas.

As Descartes wrote in his *Discourse on Method* "one cannot conceive anything so strange and so implausible that it has not already been said by one philosopher or another." As such, in relation to the treatment of the subject in the paragraphs below, a claim of pure originality would be absurd. Nevertheless, the material is wholly original in the sense that key concepts are developed in a unique manner along with all pertinent formulas, representative design parameters and technology curves so that it forms a coherent and compact reference to be used in basic engineering analysis of gas turbine combined cycles. Even then, it must be pointed out that a similar treatment can be found in the excellent brief chapter on gas turbines written by Haselbacher cited in Ref. [26]. Another valuable short reference

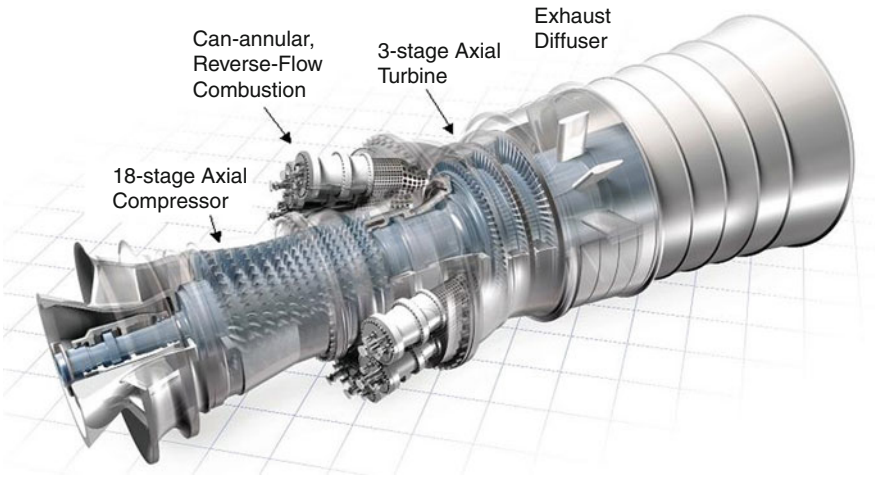

Fig. 15.6 Modern heavy-duty industrial gas turbine (Courtesy: GE Energy)

incorporating the basic fundamental considerations is cited in Ref. [24]. The treatment herein focuses on land-based heavy-duty industrial gas turbines. For a brief introduction to thermodynamic and economic considerations pertaining to aeroderivative gas turbines and pertinent references, the reader should consult Horlock [27].

Basic Thermodynamics

Gas turbine is a relatively simple turbomachine comprising three key components: Compressor, combustor, and expander (Fig. 15.6). The last one is commonly referred to as a turbine. The compressor and expander are connected through a common shaft. The operation of a gas turbine is described by a thermodynamic cycle comprising four processes: compression, heat addition or combustion, expansion, and heat rejection. A gas turbine can also be classified as an internal combustion engine (just like a car engine), in which the compressed working fluid, i.e., air, mixes with fuel, and the products of the ensuing chemical reaction (i.e., combustion) expand through the turbine. In land-based electric power generation applications, part of the useful mechanical or shaft work, produced by the expanding combustion products (approximately 50% of the total) is consumed by the compressor. The remainder is converted into electric power in a synchronous alternating current (ac) generator, which is connected to the same shaft as the gas turbine. In aircraft propulsion applications, the entire shaft work generated in the turbine is utilized to drive the engine compressor and fan. The thermal energy in

the exhaust gas is converted into kinetic energy in the exhaust nozzle, which generates the net engine thrust.

The thermodynamic cycle that describes the gas turbine operation is the *Brayton* cycle. For simple analytical calculations, which can be found in elementary textbooks on thermodynamics, the ideal or *air-standard* Brayton cycle is used. The classical (and, from an engineering perspective, the most logical) representation of the air-standard Brayton cycle is on a temperature–entropy or T-s surface as illustrated in Fig. 15.7. The key assumptions in air-standard cycle analysis are:

1. The working fluid is air, which is a calorically perfect gas (i.e., c_p = constant).
2. Isentropic (i.e., adiabatic and reversible) compression and expansion.
3. Constant pressure heat addition and heat rejection.

The two key nondimensional performance metrics for a gas turbine are specific *net* power output and thermal efficiency:

$$w = \frac{\dot{W}_{net}}{\dot{m} \cdot c_p \cdot T_1} \tag{15.1}$$

$$\eta = \frac{\dot{W}_{net}}{\dot{Q}_{in}} \tag{15.2}$$

The net power output is the difference between the compressor power consumption and the expander power production. In graphical terms, it is exactly equal to the area encompassed by the cycle 1-2-3-4-1 on the T-s diagram in Fig. 15.7. Each component's power can be calculated by the application of the *first law of thermodynamics* for steady-state steady-flow (SSSF) successively to their respective *control volumes*:

$$\dot{W}_{comp} = \dot{m} \cdot c_p \cdot (T_1 - T_2) \tag{15.3}$$

$$\dot{W}_{turb} = \dot{m} \cdot c_p \cdot (T_3 - T_4) \tag{15.4}$$

$$\dot{W}_{net} = \dot{W}_{turb} + \dot{W}_{comp} \tag{15.5}$$

From Fig. 15.7 and (Eqs. 15.3 and 15.4) one can easily see that the compressor power consumption is a *negative* number (i.e., work done *on* the control volume) and expander power generation is a *positive* number (i.e., work done *by* the control volume). Application of the first law for SSSF to the heat addition and heat rejection processes, one gets

$$\dot{Q}_{in} = \dot{m} \cdot c_p \cdot (T_3 - T_2) \tag{15.6}$$

$$\dot{Q}_{out} = \dot{m} \cdot c_p \cdot (T_1 - T_4) \tag{15.7}$$

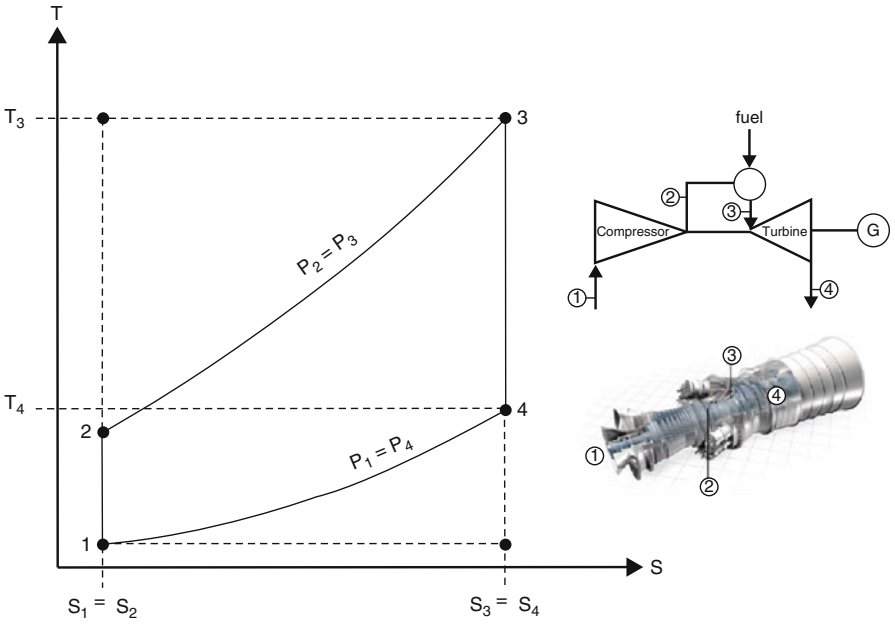

Fig. 15.7 Temperature–entropy diagram of gas turbine Brayton cycle

From Fig. 15.7 and (Eqs. 15.6 and 15.7), the heat input to the cycle is a *positive* number (i.e., heat supplied *to* the control volume) and heat rejection from the cycle is a *negative* number (i.e., heat taken *from* the control volume).

In addition to the first law of thermodynamics for a SSSF process (or control volume analysis), there is one more key thermodynamic relationship that forms the heart of the GT Brayton cycle calculations: pressure–temperature ratio for an isentropic process:

$$\frac{T_2}{T_1} = \left(\frac{p_2}{p_1}\right)^{\frac{\gamma-1}{\gamma}} \tag{15.8}$$

where γ is the ratio of constant pressure and constant volume-specific heats. Combining (Eqs.15.1–15.7), in nondimensional terms and applying the isentropic formula in Eq. (15.8) to compression and expansion processes, one ends up with the following two expressions:

$$w = \left(\pi^k - 1\right) \cdot \left(\frac{\tau_3}{\pi^k} - 1\right) \tag{15.9}$$

$$\eta = 1 - \frac{1}{\pi^k} \tag{15.10}$$

where $\pi = p_2/p_1$ is the cycle pressure ratio, τ_3 is the cycle maximum temperature (nondimensionalized via division by T_1) and k is the isentropic exponent, $\gamma - 1/\gamma$. The two simple formulas, Eqs. (15.9) and (15.10), which are strictly valid only for an ideal air-standard cycle, illustrate almost all of the key facts concerning gas turbine performance:

1. Gas turbine or Brayton cycle performance is controlled by two parameters: Cycle pressure ratio, π, and maximum cycle temperature, τ_3.
2. Cycle efficiency is a function of cycle pressure ratio only; higher cycle pressure leads to higher cycle efficiency.
3. Higher cycle temperature leads to higher cycle specific output.
4. Higher cycle pressure ratio, beyond a certain value, is detrimental to cycle specific output (i.e., $\frac{\partial^2 w}{\partial \pi^2} < 0$ and $\pi = \sqrt[2k]{\tau_3}$ for $\partial w/\partial \pi = 0$).

These observations are also borne out qualitatively by a close examination of the cycle T-s diagram in Fig. 15.7. As the heat addition isobar moves upward (i.e., higher cycle pressure ratio, π) one can visually verify that the area encompassed by the cycle, 1-2-3-4-1, becomes smaller until, in the limit, it becomes zero. Equation (10) numerically implies that, in the limit when π is sufficiently high, the cycle efficiency will approach 100%, or, $\eta \to 100\%$ as $\pi \to \infty$. This, of course, is impossible, because, as dictated by the *second law of thermodynamics*, the maximum theoretical efficiency attainable by any cycle is given by the Carnot cycle efficiency. The Carnot cycle is a hypothetical power cycle that is represented by two isentropic processes, i.e., compression and expansion; and two isothermal processes, i.e., heat addition and heat rejection. Graphically, it is the rectangle enveloping the Brayton cycle, which is bounded by T_1 and T_3 isotherms and s_1 and s_3 isentropes.

For the cycle in Fig. 15.7, one can easily visualize the limit of $\pi \to \infty$ as T_3 stays constant. In the limiting case, one will end up with a Brayton cycle that is a rectangle with $\sim$0 area (i.e., zero specific output) and heat addition and rejection at constant temperatures T_3 and T_1, respectively, which essentially defines a Carnot cycle with the efficiency

$$\eta = 1 - \frac{T_1}{T_3} \tag{15.11}$$

Comparing with Eq. (15.10), for a cycle maximum temperature of $T_3 = 1{,}500°C$ and $\gamma = 1.4$, this would correspond to a cycle pressure ratio of $\pi = 577$ and cycle efficiency $\eta = 87.4\%$. In other words, as dictated by the second law of thermodynamics, the maximum theoretical cycle efficiency that is attainable by a gas turbine with a "firing temperature" of 1,500°C is 87.4%. Clearly a cycle pressure ratio of 577 is of little practical interest. For the modern heavy-duty industrial gas turbines, the typical value of π is about 18. What does the second law say about a gas turbine for a cycle maximum temperature of $T_3 = 1{,}500°C$ and $\pi = 18$? In order to find that

out, consider the isobaric heat addition process 2 → 3 in Fig. 15.7. For a reversible and isobaric process, the modified Gibbs equation is

$$h_3 - h_2 = \int_2^3 T \cdot ds \tag{15.12}$$

One can imagine an (hypothetical) isothermal process that takes place at a constant temperature, whose value lies between T_3 and T_2, and has the same entropy as the actual end states 2 and 3. This process would have exactly the same numerical value of heat addition as the original process, i.e., h_3– h_2, per unit mass. For that process, Eq. (15.12) can be rewritten as

$$h_3 - h_2 = \bar{T}_{\mathrm{H}} \cdot (s_3 - s_2) \tag{15.13}$$

Using the calorically perfect gas relationships, the *mean-effective* heat addition temperature can be found from Eq. (15.13) as

$$\bar{T}_{\mathrm{H}} = \frac{T_3 - T_2}{\ln\left(\frac{T_3}{T_2}\right)} \tag{15.14}$$

Using the same logic, the mean-effective heat rejection temperature is calculated as

$$\bar{T}_{\mathrm{L}} = \frac{T_4 - T_1}{\ln\left(\frac{T_4}{T_1}\right)} \tag{15.15}$$

These two mean-effective temperatures are graphically depicted in Fig. 15.8. Thus, qualitatively any thermodynamic cycle in general, and the Brayton cycle in particular, 1-2-3-4 in Fig. 15.8, can be represented by its *Carnot-equivalent* cycle, 1′-2′-3′-4′, with mean-effective (constant) heat addition and heat rejection temperatures that are given by Eqs. (15.14 and 15.15). The efficiency of that cycle would be given by the well-known relationship for the Carnot efficiency, i.e.,

$$\eta = 1 - \frac{\bar{T}_{\mathrm{L}}}{\bar{T}_{\mathrm{H}}} \tag{15.16}$$

For an ideal air-standard Brayton cycle, one can show that Eq. (15.16) is the same as Eq. (15.10). Thus, for any gas turbine with a cycle pressure ratio of 18, the maximum theoretical efficiency is 56.2%. Using Eqs. (15.8), (15.14), and (15.15), this would be the efficiency of a Carnot cycle with isothermal heat addition and heat rejection at 852°C and 219°C, respectively. It is interesting to note that, changing the cycle maximum temperature from 1,500°C to 1,400°C would change these temperatures to 814°C and 203°C, respectively, but would *not* change the cycle efficiency, i.e., 56.2%, which is only a function of π. This is in contrast to the

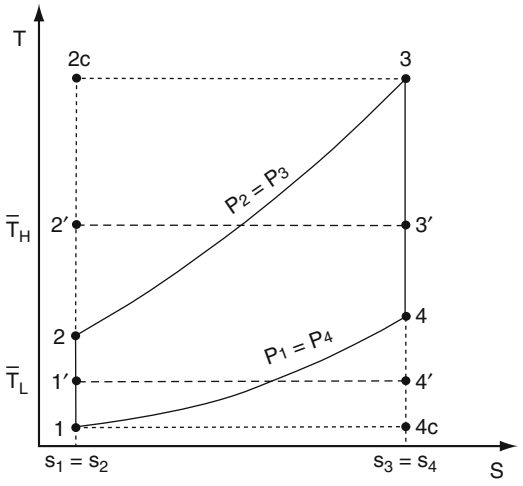

Fig. 15.8 Temperature–entropy diagrams of gas turbine Brayton cycle and its "Carnot equivalent"

performance trend of the "real" gas turbines, whose thermal efficiency does indeed increase with increasing cycle maximum or *firing* temperature. Why this is so will be understood below.

One key observation from Fig. 15.8 is the large thermal efficiency gap between the ultimate Carnot efficiency given by Eq. (15.11) and the maximum theoretical entitlement level as dictated by the second law, Eq. (115.0) or Eq. (15.16), which is nearly 30 percentage points. Graphically, this gap is represented by the two triangular areas in Fig. 15.8:

1. The upper triangular area 2-2c-3-2, which is equal to the rectangular area 2′-2c-3-3′-2′, and represents the heat addition (i.e., combustion) irreversibility
2. The lower triangular area 1-4-4c-1, which is equal to the rectangular area 1-1′-4′-4c-1, and represents the irreversibility and exergy loss via heat rejection to a heat sink

In terms of cycle temperatures, the upper triangular area is quantified by the gap between the cycle maximum temperature, T_3, and the mean-effective heat addition temperature $\bar{T}_H$. Similarly, the lower triangular area is quantified by the gap between the cycle minimum or ambient temperature, T_1, and the mean-effective heat rejection temperature $\bar{T}_L$. The latter mechanism of "lost work" associated with heat rejection also points the way to the gas and steam turbine combined cycle power plant concept. This will be explored in some more detail later in the discussion.

The real gas turbine Brayton cycle differs from the ideal, air-standard cycle in the following respects:

1. Non-isentropic compression and expansion (represented by component polytropic or isentropic efficiencies)
2. Pressure losses during heat addition and heat rejection

3. Real gas effects (represented by a suitable equation of state)
4. Change in working fluid composition and properties downstream of combustion process

These nonidealities can be easily incorporated into the simple equations above via polytropic component efficiencies, pressure loss factors, and real gas equation of state. One can refer to one of the available textbooks on the subject for details, e.g., Ref. [29]. For example, Eq. (15.9) can be rewritten as

$$w = \left(1 - \pi_c^{\frac{k_a}{\eta_c}}\right) + (1+f)\cdot\chi_g\cdot\tau_3\cdot\left(1 - \frac{1}{\pi_t^{\eta_t\cdot k_g}}\right) \tag{15.17}$$

where π_c and $\pi_t < \pi_c$ are compressor and turbine pressure ratios, respectively, k_a and k_g are isentropic exponents for air and combustion products, respectively, and η_c and η_t are compressor and turbine polytropic efficiencies, respectively. The ratio of the specific heats of combustion products and air is χ_g and f is the fuel–air mass flow ratio. Heat addition can be found from the fuel consumption, i.e.,

$$\dot{Q}_{in} = \dot{m}_f \cdot \mathrm{LHV} \tag{15.18}$$

where LHV is the net or lower heating value of the fuel at the reference temperature, T_{ref}. The efficiency of the gas turbine is the ratio of Eqs. (15.17) and (15.18), i.e.,

$$\eta = \frac{\left(1 - \pi_c^{\frac{k_a}{\eta_c}}\right) + (1+f)\cdot\chi_g\cdot\tau_3\cdot\left(1 - \frac{1}{\pi_t^{\eta_t\cdot k_g}}\right)}{f\cdot\ell} \tag{15.19}$$

where ℓ is the nondimensional fuel energy content, $\mathrm{LHV}/c_{p,a}\cdot T_1$. Note that for clarity, mechanical and electric losses are omitted from Eqs. (15.17) and (15.19), which represent the "shaft" performance. Typically quantified via mechanical and generator efficiencies, η_m and η_g, respectively, these losses should be accounted for the gas turbine generator's net electric output. The fuel mass flow rate (as a fraction of turbine airflow) that is requisite for a specified cycle maximum temperature is given by

$$f = \frac{\chi_g\cdot(T_3 - T_{ref}) - (T_2 - T_{ref})}{\ell\cdot T_1 + \chi_f\cdot(T_f - T_{ref}) - \chi_g\cdot(T_3 - T_{ref})} \tag{15.20}$$

where the second term in the denominator is the sensible fuel energy input and χ_f is the ratio of the specific heats of fuel and air. Comparing Eq. (15.19) (along with Eq. (15.20) that sets the denominator) with Eq. (15.10), one can easily observe that the GT thermal efficiency, when accounting for the "real" cycle effects, is indeed a function of τ_3. While it is difficult to discern the impact of τ_3 on η just by looking at Eqs. (15.19) and (15.20), a sample calculation can illustrate that as shown in Fig. 15.9.

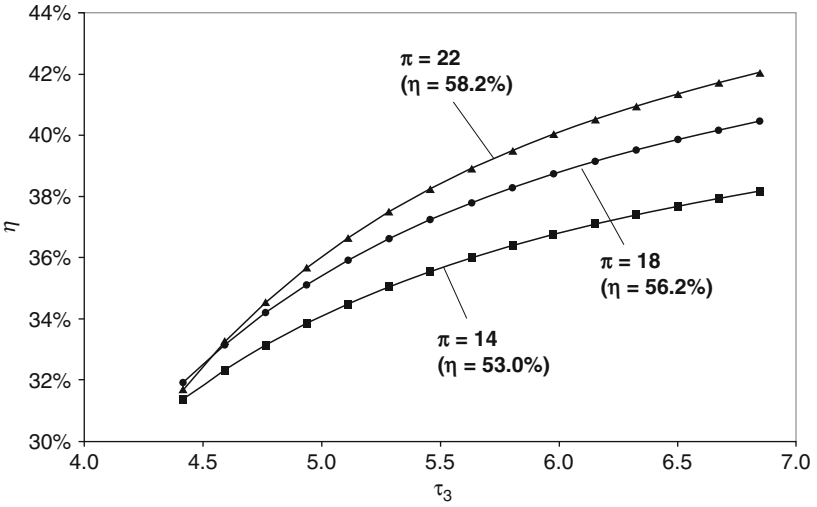

Fig. 15.9 Real Brayton cycle efficiency from Eqs. (15.19) and (15.20) as a function of cycle pressure ratio (π) and maximum cycle temperature (τ_3). Also shown (in parentheses) are the ideal, air-standard cycle efficiencies from Eq. (15.10)

Typical values that are reasonably accurate for gas turbines burning natural gas fuel (assumed to be 100% CH_4 or methane) are given below (adopted from Ref. [29]) and used in the calculations that resulted in the curves depicted in Fig. 15.9:

LHV = 21,515 Btu/lb
$c_{p,a}$ = 0.24 Btu/lb-R (1.005 kJ/kg-K)
$c_{p,g}$ = 0.274 Btu/lb-R (1.148 kJ/kg-K) or χ_g = 1.1417
$c_{p,f}$ = 0.60 Btu/lb-R (2.5125 kJ/kg-K) or χ_f = 2.50
γ_a = 1.400
γ_g=1.333
η_c = 87.8%
η_t = 85%
η_m = 99%
η_g = 98.9%
k_a = 0.2857
k_g = 0.2498
T_{ref} = 77°F (25°C)
ℓ = 172.728

Original equipment manufacturer (OEM) data for five 50-Hz (3,000 rpm) heavy-duty industrial gas turbines from a recent trade publication [6] are given in Table 15.2.

For an actual gas turbine, the cycle maximum temperature T_3 is equivalent to the turbine inlet temperature (TIT) at the exit of the gas turbine combustor. Another value that is frequently used in the industry is the "firing temperature," which is the temperature at the stage-1 blade row (rotor) inlet. This temperature, also known as

Table 15.2 OEM data for 50-Hz heavy-duty industrial gas turbines [6]. The maximum cycle temperature, T_3, values are estimated using the published output, efficiency, pressure ratio (PR), and exhaust data with Eqs. (15.17–15.20)

	T_3						Exhaust	
Turbine	(°C)	°F	PR	PR_t	Output (MW)	Eff.	(kg/s)	°C
A	1,415	2,579	17.7	15.9	285.0	39.6%	690	572
B	1,443	2,629	17.0	13.5	255.6	36.9%	641	602
C	1,501	2,734	18.3	14.5	279.2	37.8%	655	629
D	1,435	2,616	18.2	16.3	292.0	39.8%	692	577
E	1,476	2,688	18.0	15.5	312.1	39.3%	720	597

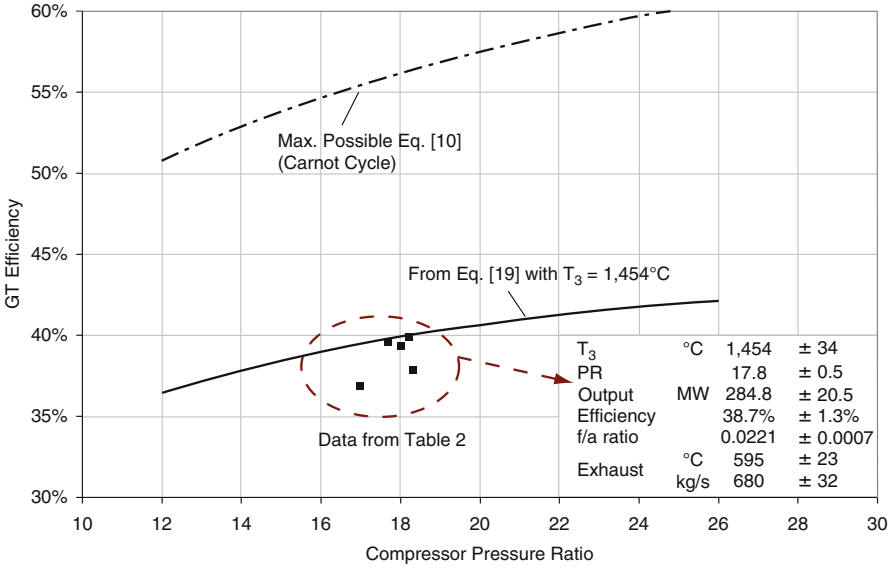

Fig. 15.10 Gas turbine efficiency from Eq. (15.19) as a function of compressor PR (Data is from Ref. [6] and summarized in Table 15.2)

rotor inlet temperature (RIT) is the maximum temperature at which the combustion products start producing useful expansion work. The difference between TIT and RIT is about 250°F for modern air-cooled gas turbines and reflects the dilution effect of the stage-1 nozzle and forward wheel space cooling flow. One other cycle maximum temperature definition, favored by European OEMs, is the ISO-TIT, which is a fictitious number as defined by ISO-2314 (typically ~180°F lower than RIT). Obviously, for an uncooled turbine all these definitions are the same.

Gas turbine efficiency as a function of PR is shown in Fig. 15.10. Specific output, w, in the range covered by the turbines in Table 15.2 is 400–450 kJ/kg. Carbon dioxide emissions are calculated from the airflow and fuel flow using chemical reaction equations for 100% CH_4 gaseous fuel assumption as 510 kg/h per MW of output at 39% net efficiency. Each one percentage point improvement in efficiency

is worth about 15 kg/h per MW reduction in CO_2 emissions. This is equivalent to 27,000 metric tons for a 300 MW GT running at base load for 6,000 h/year.

Figure 15.10 shows that the gap between the current State of the Art (SOA) in gas turbine technology and the maximum theoretical entitlement level, as dictated by the second law, is more than 15 efficiency points. The GT efficiency – compressor pressure ratio (PR) trend in Fig. 15.10 (via Eq. (15.19)) gives the impression that, for a given cycle maximum temperature, the efficiency can be improved indefinitely by increasing the PR. This is *not* true due to a key feature of modern gas turbines that is very difficult to capture in simplified models such as Eqs. (15.17–15.20): turbine hot gas path (HGP) component cooling via air extracted from the compressor discharge and/or interstage locations. Since the early days of GT development, the components exposed to the highest temperature environment have been cooled with air drawn from the compressor. The Junkers Jumo-004 jet engine of the German fighter plane Messerschmitt 262, which entered active service in 1944 during the last stages of the World War II, was the first mass production turbojet engine in the history with a turbine inlet temperature (TIT) of 1,427°F [13]. The hollow turbine blades (manufactured by folding flat sheets of 12% Cr alloy called *Cromadur*) were cooled by air extracted from between the fourth and fifth stages of the compressor and introduced to the blade through the holes drilled into the disk. The cooling technology, although unchanged in basic principles, has advanced greatly over the years with the introduction of complex serpentine cooling passages, impingement, film, and transpiration cooling techniques; paced by concurrent advances in superalloys (e.g., nickel-based directionally solidified or single-crystal), manufacturing techniques (e.g., investment casting), oxidation/corrosion (e.g., MCrAlY), and thermal barrier (e.g., yttria-stabilized zirconia, YSZ) coatings. This development supported the advances in TIT, which nearly doubled the standard set by Jumo-004 over the course of the next 50 years (e.g., see Fig. 15.11 that uses data from Cumpsty [30]). A good overview of the current SOA in advanced GT materials and coatings can be found in Ref. [31].

An alternative to open loop air-cooling (OL-AC) has recently been commercially introduced at the 480-MW Baglan Bay 109H CC power plant in Wales [32]. This machine employs closed-loop steam cooling (CL-SC) for the majority of the turbine HGP components (the first two stages of the four-stage turbine, to be exact). A "lighter" version of the H-System™ is the G-Class turbine with steam cooling limited to the stationary parts upstream of the turbine HGP [33].

A structural refinement to the basic GT Brayton cycle is the inclusion of a second "reheat" combustor within the turbine expansion. Reheat, or *sequential combustion* as it is referred to by the OEM that successfully commercialized the technology increases the mean-effective cycle heat addition temperature and reduces the combustion irreversibility [34] (the upper triangular area 2-2c-3-2 in Fig. 15.3). From a fundamental thermodynamic perspective, lower combustion losses give the GT cycle with reheat combustion a higher performance entitlement than a cycle without it. Similarly, there is no doubt that closed-loop (external) cooling is superior to open-loop (internal) cooling but the exact magnitude of that advantage in real machines is difficult to quantify. Chiesa and Macchi [35] quantified the

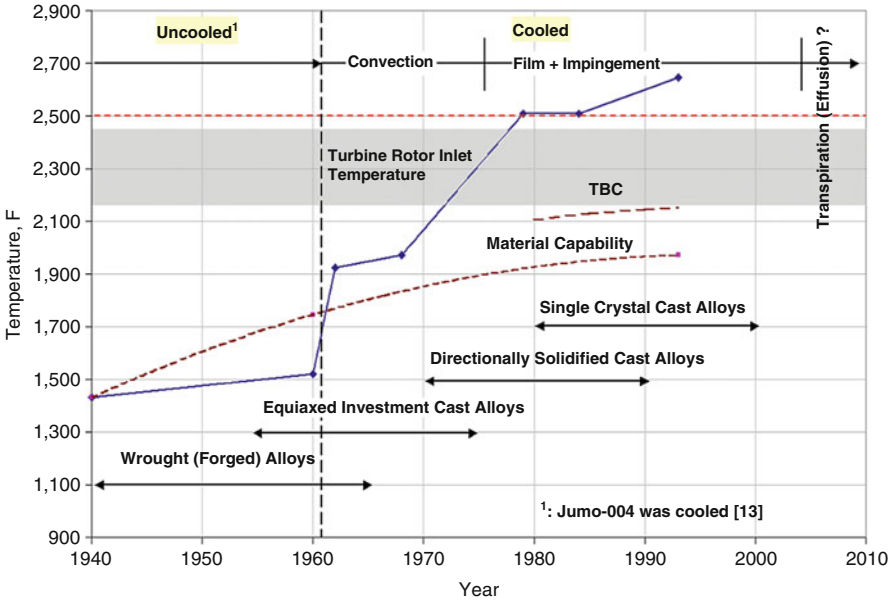

Fig. 15.11 Turbine RIT and bucket alloy capability history [30]. One can add ~250°F to RIT to get a rough idea about TIT of the advanced F-Class units. The shaded region designates the melting point of nickel-based superalloys

Table 15.3 Comparison of CC performances based on four major GT technologies [35]: Air-cooled (OL-AC), air-cooled reheat (OL-AC+SC), steam-cooled (CL-SC), and steam-cooled reheat (CL-SC+SC)

	OL-AC	OL-AC+SC	CL-SC	CL-SC+SC
GT PR	20	30	23	30
HPT RIT (°C)	N/A	1,290	N/A	1,430
HPT RIT (°F)	N/A	2,354	N/A	2,606
RIT (°C)	1,430	1,430	1,430	1,430
RIT (°F)	2,606	2,606	2,606	2,606
Net η_{CC} (%, points)	Base	+0.81	+1.77	+2.74

advantages of OL-AC (with and without reheat combustion) and CL-SC technologies via detailed calculations. Using OEM data from GE's 7FB, Siemens V94.3A (now SGT5-4000F), Alstom's GT-26, and MHI's M701G units for calibration, they have developed very detailed cooled GT models and evaluated the CC performances. Their findings are summarized in Table 15.3, which shows that CL-SC has an advantage of ~1.8 points (%) in net η_{CC} over OL-AC.

A realistic assessment of the gas turbine requires some means to incorporate the cooling penalty into the GT calculations. Cooled turbine expansion models, no matter how much simplified, involve a rather cumbersome system of equations amenable only to a numerical solution. In the open literature, there are numerous

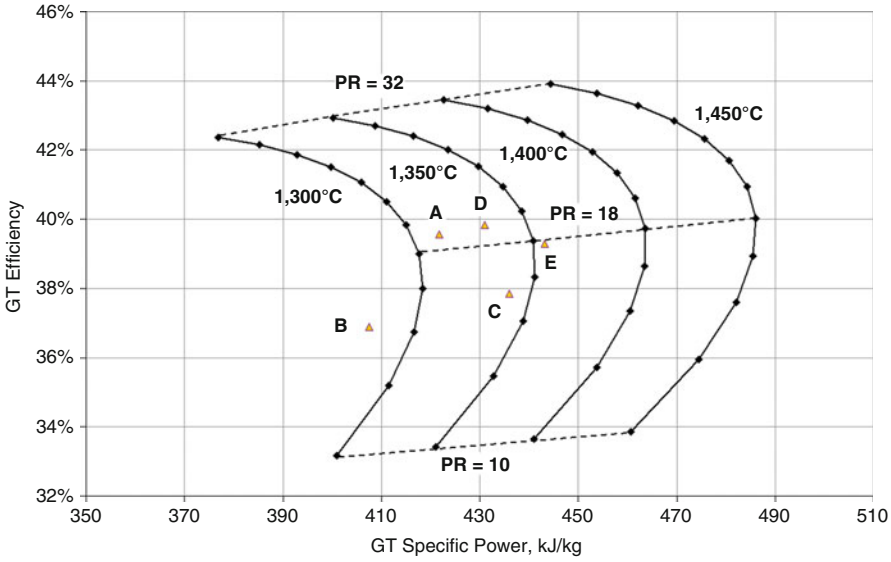

Fig. 15.12 "Real" gas turbine technology curves for different PR-RIT combinations [46] (Also shown is data from Table 15.2 (as published in Ref. [6]))

published works that range from Holland and Thake [36] and several papers by Elmasri [37–41] during 1980s to the more recent works of Horlock and coworkers [42–45]. Young and Wilcock's comprehensive study [45] and the similar treatment in Ref. [35] incorporate detailed aerothermodynamic calculations. On the business side, obviously not available for public consumption, OEMs have their own in-house proprietary codes containing the field-proven knowledge (instead of theoretical approximations) distilled from decades of experience in manufacturing and testing gas turbines. The results from a more realistic GT calculation [46], which includes the impact of turbine cooling with compressor extraction air, are shown in Fig. 15.12.

Myriad alternate GT design variations have been proposed and entered the literature, some to the extent that they are even covered in elementary textbooks; e.g., compressor intercooling, regeneration (also referred to as recuperation), a combination of both, steam injection (STIG) [47, 48], humid air turbine (HAT) [49], chemical recuperation [50], and closed cycles [51] are among the most well known. For a comprehensive look at those variants and their relative merits, as well as references to the pertinent literature, one can consult the relevant sections in Wilson and Korakianitis [11]. Intercooling and recuperation technologies have been demonstrated successfully in aeroderivative gas turbines [52,53], whereas the combination of both (ICR) has been incorporated into a ship-propulsion unit [54]. Nevertheless, steam-cooled (G- or H-Class) and reheat machines are the only two commercially proven and successful heavy-duty industrial variants of the basic air-cooled GT, which are suitable to large-scale base load electric power generation.

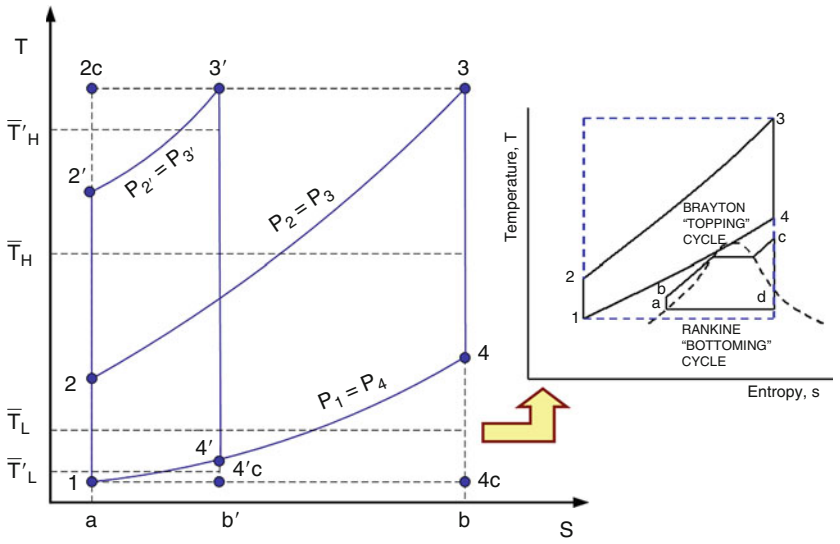

Fig. 15.13 Comparison of Brayton cycles with different PRs on a T-s diagram. Also illustrated is the "combined" cycle concept, in which the Rankine "bottoming" cycle partially recovers the Brayton "topping" cycle heat rejection "lost" work

So far it has been demonstrated that increasing the compressor PR and/or TIT (i.e., maximum cycle temperature) increases the GT efficiency and specific work. The latter reaches a maximum before further increase in PR decreases it. Furthermore, increasing TIT is favorable to CC-specific work and CC efficiency. These trends can be easily visualized and quantified by the ideal cycle diagrams shown in Fig. 15.13.

The heat rejection "lost work" quantified by the lower triangular area 1-4-4c-1 suggests that a better approximation of the Carnot cycle can be achieved by utilizing the heat source provided by the working fluid at the GT exhaust (i.e., state 4) in a second power generation cycle. At this point, the Rankine cycle presents itself as the ideal choice due to two facts:

1. Good match with GT exhaust (on average about 600°C for SOA F-Class machines) for steam generation at 125–165 bar
2. Constant temperature heat rejection (i.e., in the steam condenser) at a temperature that is much closer to T_1 than $\overline{T}_L$

Earlier in the section, it was shown that the Brayton cycle efficiency is given by the mean-effective cycle heat addition and rejection temperatures, $\overline{T}_H$ and $\overline{T}_L$, respectively, e.g., Eq. (15.16). Increasing the cycle maximum pressure from p_2 to p_2' increases the cycle efficiency by simultaneously increasing $\overline{T}_H$ and reducing $\overline{T}_L$. It is easy to see that the cycle-specific work, quantified by the area 1-2-3-4, would go through a maximum before approaching zero at which point the cycle efficiency

is the Carnot efficiency. The ultimately detrimental effect of continuously increasing the Brayton "topping" cycle (BTC) PR on CC efficiency can also be seen from Fig. 15.13. The maximum possible CC "bottoming" cycle work, limited by the second law, is equal to the triangular area 1-4-4c-1, which can be shown to be exactly equal to the GT exhaust gas exergy [55]. It is easy to visually appreciate the steady reduction in this maximum with increasing PR (cf. 1-4-4c-1 and 1-4′-4′c-1). The efficiency of the ideal Rankine bottoming cycle (RBC) is given by the equation below:

$$\eta_{\mathrm{RBC}} = 1 - \frac{T_1}{\bar{T}_{\mathrm{L}}} \tag{15.21}$$

where $\bar{T}_{\mathrm{L}}$ is from Eq. (15.15). The formula in Eq. (15.21) clearly implies that this particular ideal Rankine cycle would be equivalent to a Carnot engine operating between the temperature reservoirs at $\bar{T}_{\mathrm{L}}$ and T_1. Furthermore, the product of Eq. (15.21) and the total energy content of the GT exhaust $\dot{Q}_{\mathrm{exh}}$ can be shown to be exactly equal to the total exergy of the exhaust gas [55]. Exergy is a fluid property that can be calculated using a suitable equation of state with two other known properties (e.g., pressure and temperature) and the composition.

By looking at the cycle T-s diagram in Fig. 15.13, the ideal CC efficiency with ideal Brayton and Rankine cycles can be deduced to depend on the ratio of the mean-effective Brayton cycle heat addition temperature given by Eq. (14) and the ambient temperature T_1, i.e.,

$$\eta_{\mathrm{CC}} = 1 - \frac{\ln\left(\frac{\tau_3}{\pi^k}\right)}{\tau_3 - \pi^k} \tag{15.22}$$

Ignoring the miscellaneous topping and bottoming cycle losses and minor inputs, a simplified version for the CC shaft efficiency can also be written as

$$\eta_{\mathrm{CC}} = \eta_{\mathrm{BTC}} + (1 - \eta_{\mathrm{BTC}}) \cdot \eta_{\mathrm{RBC}} \tag{15.23}$$

Taking the derivative of both sides with respect to the PR and setting the CC efficiency derivative to zero for the maximum, one finds that (note that the RBC and BTC efficiencies are approximately the same in magnitude)

$$\frac{\partial \eta_{\mathrm{BTC}}}{\partial \mathrm{PR}} \approx -\frac{\partial \eta_{\mathrm{RBC}}}{\partial \mathrm{PR}} \tag{15.24}$$

This relationship states that the maximum *Brayton–Rankine* combined cycle efficiency occurs at the point where the rate of increase of BTC efficiency with PR is the same as the rate of decrease of the RBC efficiency. Using the ideal Brayton cycle formulas, which can be found in any standard thermodynamics textbook such as Ref. [28], the rate of increase of BTC efficiency with increasing PR is

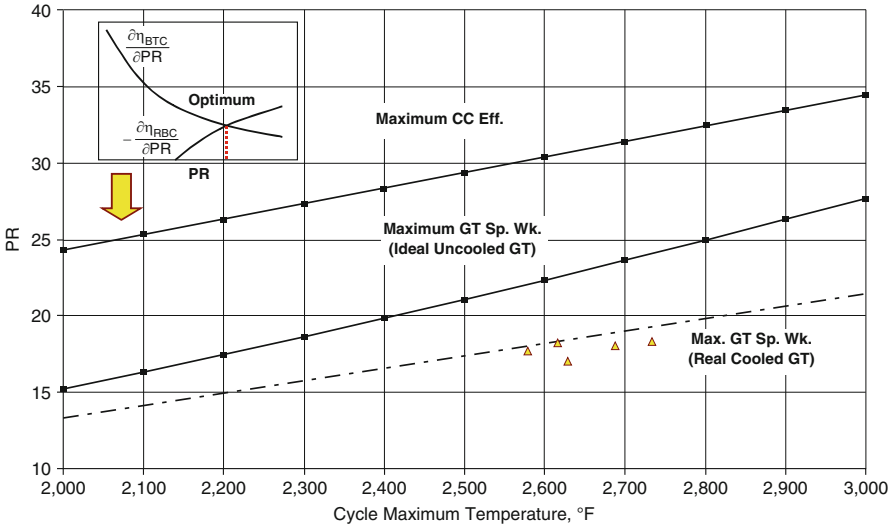

Fig. 15.14 PR for maximum CC efficiency and maximum BTC specific work. Data points are from Ref. [6]. Cycle maximum temperature or T_3 values are from Table 15.2. The inset illustrates the calculation of maximum η_{CC} point using Eqs. (15.24–15.26)

$$\frac{\partial \eta_{BTC}}{\partial PR} = \frac{\gamma - 1}{\gamma} \cdot PR^{\frac{1-2\gamma}{\gamma}} \tag{15.25}$$

From Eq. (15.21), once again using the ideal Brayton cycle relationships, the rate of decrease of the RBC efficiency with increasing PR is found as

$$\frac{\partial \eta_{RBC}}{\partial PR} = \frac{\gamma - 1}{\gamma} \cdot \frac{\left(\frac{T_1}{T_L}\right) \cdot \left(\frac{T_4}{T_L} - 1\right)}{PR \cdot \ln\left(\frac{T_4}{T_1}\right)} \tag{15.26}$$

Combining Eqs. (15.21–15.26) with $\gamma = 1.4$ and $T_1 = 85°F$ (assuming RBC heat rejection at 1.2 in. Hg or 41 mbar of steam condenser pressure) and solving them numerically, the PR of the BTC for maximum CC efficiency can be plotted as a function of T_3 (see Fig. 15.14). Also plotted in Fig. 15.14 is the PR corresponding to the maximum BTC specific work, $\pi = \sqrt[2\gamma]{\tau_3}$, with T_1=59°F. For comparison, representative OEM data extracted from a recent trade publication [6] is also shown. It is interesting to note the excellent agreement of the PR-TIT data of actual production machines with values corresponding to maximum GT-specific power output predicted using a rigorous cooled gas turbine model.

Using an uncooled *quasi-ideal* GT model with reasonable assumptions outlined earlier in the section to take into account the real turbine losses, CC efficiencies

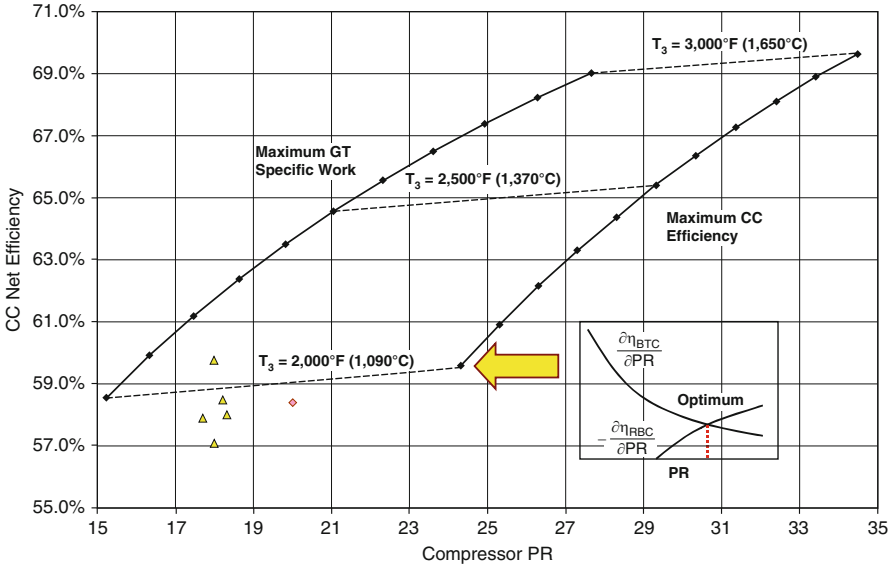

Fig. 15.15 Uncooled GT-based CC efficiencies (note that $T_3 \equiv$ TIT). The data (symbol Δ) is from Table 15.4. The other data is from Ref. [35] for the SOA air-cooled GT (TIT=2,826°F). The inset illustrates the calculation of maximum η_{CC} point using Eqs. (15.24)–(15.26) in the text. Component polytropic efficiencies are assumed to be 92.5% and 90% for the compressor and turbine, respectively

corresponding to the parameters in Fig. 15.14 are calculated and plotted in Fig. 15.15. The key takeaways from the plots in those figures are rather illuminating:

1. Actual OEM designs are at PR values somewhat lower than those for maximum GT-specific output in an uncooled GT but coincide extremely well with the air-cooled GT specific work line, in accordance with the earlier observation made by Horlock [24].
2. This seems to be a reasonable choice from a cost perspective with ∼0.50 percentage points sacrifice in performance vis-à-vis the maximum η_{CC} that has a ∼50% larger PR. In fact, the proximity of the two maxima is even closer in the presence of turbine cooling so that this is a very reasonable trade-off indeed.
3. 65% and 70% net CC efficiencies require uncooled turbines with TIT of 2,500°F and 3,000°F, respectively.

OEM data for combined cycle performances based on five 50-Hz (3,000 rpm) heavy-duty industrial gas turbines from a recent trade publication [6] (see Table 15.2) are given in Table 15.4. The data is for two major combined cycle configurations, which are labeled as 1 × 1 (i.e., one GT and one ST) and 2 × 1 (i.e., two GTs and one ST). Using the GT performance in Fig. 15.12 as a basis, CC performance curves can be developed using the exergy-based bottoming cycle calculations in Ref. [56] (see Fig. 15.16).

Table 15.4 OEM data for combined cycle performances (1×1 and 2×1) of 50-Hz heavy-duty industrial gas turbines [6] (Gas turbine data is in Table 15.2)

		1×1			2×1		
	GT	ST	CC		ST	CC	
Turbine	MW	MW	MW	η (%)	MW	MW	η (%)
A	285.0	141.0	415.1	57.9	282.0	830.2	57.9
B	255.6	141.8	390.8	56.7	289.2	786.9	57.1
C	279.2	157.9	412.9	58.0	315.3	825.4	58.0
D	292.0	144.7	423.0	58.4	290.3	848.0	58.5
E	312.1	157.3	459.0	59.5	317.7	921.1	59.7

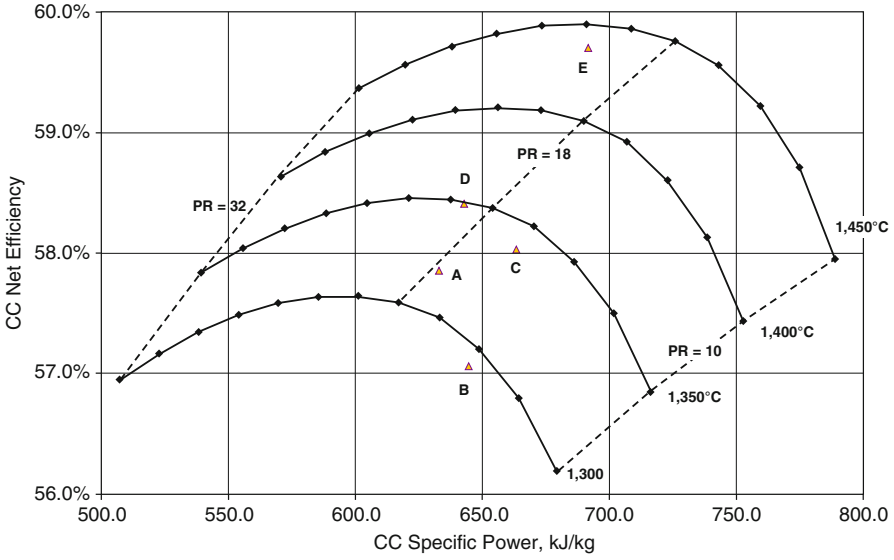

Fig. 15.16 "Real" combined cycle technology curves for different PR-RIT combinations. They are based on the gas turbine technology curves in Fig. 15.12. (Also shown is data from Table 15.4 (as published in Ref. [6]))

Today's SOA in CC performance with advanced gas turbines corresponds to a range of 57% to ~60% with TIT values in the range of 2,600–2,800°F. This is a far cry from the theoretically possible values in the absence of turbine cooling as shown in Fig. 15.15 (by about 10 percentage points). Sponsored by the DOE's National Energy Technology Laboratory (NETL), the *Vision 21* program has a goal to develop, by 2015, the core modules for a fleet of fuel-flexible, multiproduct energy plants that boost power efficiencies to more than 60% (75% on an LHV basis for gas-fueled plants), emit virtually no pollutants, and with carbon sequestration release minimal or no carbon emissions. Lately, several published claims about the future of the CC plant performance at the end of the first quarter of the twenty-first century stated a goal of 65% with the possibility of over 70% with an air-cooled GT [57]. The uncooled GT–based CC efficiency curves and the current SOA data in Fig. 15.15

underline the significant hurdles to be overcome in terms of cooling flow reduction in pace with increasing firing temperatures in order to achieve those goals. The gap between the uncooled GT TIT (i.e., same as RIT) requirement for 65% η_{CC} and the current material capability is nearly 800°F (~450°C). The current trend in superalloy capabilities, considering the competing tendencies in strength (i.e., creep rupture and fatigue limits) and corrosion resistance, does not seem to be likely to alleviate too much of that [58]. A combination of advanced materials including ceramic matrix composites, metal foams (to enable the upper limit of film cooling, i.e., effusion or transpiration cooling) [59] and external cooling (most likely via steam) accompanied by bottoming cycle advances is imperative to even approach the stated efficiency goals with acceptable NO_x and CO emissions. It is thus fairly obvious that a η_{CC} goal of 65% and higher in a *Brayton–Rankine* CC power plant is a highly unlikely proposition in near future. This is more or less the conclusion reached by Rao et al. [60] who investigated the plant system configurations that might be able to meet the performance and emission goals of Vision 21 program. They concluded that hybrid systems integrating fuel cells with gas turbines, e.g., SOFC/GT hybrid system [61], were required to meet the program goals. There's little doubt about the very attractive efficiency of the SOFC/GT hybrid systems, e.g., 65–70% for atmospheric cells and 74–76% for pressurized cells [62]. What is really doubtful is whether they will be competitive with gas turbine–based systems for large-scale electric power generation considering their low power density, e.g., less than 5 kW/m^2 (cf. ~3,000 kW/m^2 for a large GT), and high cost, e.g., about $1,500/kW to $3,000/kW in 2010 dollars [63] (cf., $350/kW to $500/kW for a GT depending on its size).

Today's SOA in CC Power Plants

A schematic diagram of a CC system is shown in Fig. 15.17, which depicts the four major components: gas turbine, steam turbine, condenser, and the heat recovery steam generator (HRSG). Not shown is the cooling tower (CT), which cools the condenser cooling water. Usually, the heat rejection system (including condenser, CT and circulation pump), and feed pumps along with myriad smaller heat exchangers (such as the GT fuel gas heater in the upper left corner in Fig. 15.17) are collectively referred to as the "balance of plant" (BOP).

The equipment that combines the GT (i.e., Brayton cycle) and ST (i.e., Rankine cycle) is the HRSG. Hot GT exhaust gas (>1,100°F for modern F-Class units) transfers heat to condensate and generates superheated steam, typically at multiple pressure levels, which is used in the ST for power generation. Current SOA is a three-pressure system with reheat (i.e., heating of HP steam turbine exhaust, referred to as "cold reheat," to the same temperature as the main or HP steam) with steam temperatures of 1,050°F or higher. Highest steam pressure at the ST inlet (throttle) is around 1,800–2,500 psia, beyond which the pressures at the generation point in the HRSG exceed the critical pressure and one would require a "once-through" steam generation system as opposed to the existing "drum type"

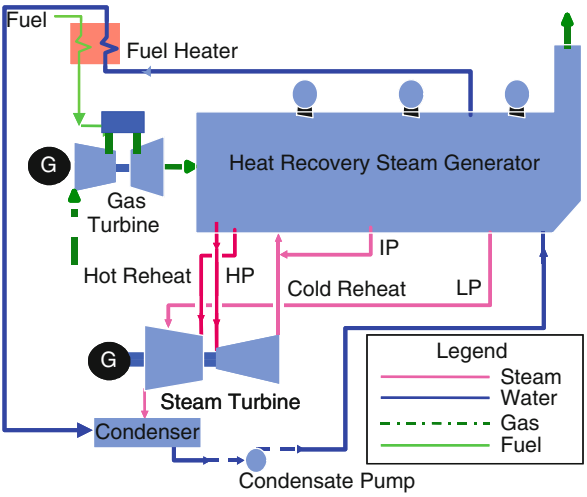

Fig. 15.17 Three-pressure, reheat (3PRH) combined cycle diagram (Source: GE Energy [64])

system. From the fundamental thermodynamics discussed earlier, the theoretically maximum (net) power output that can be obtained from the Rankine bottoming cycle of the CC plant is exactly equal to the exergy of the GT exhaust gas [55]. Today's most advanced plants with advanced F-, G-, and/or H-Class GTs and 3PRH steam systems, are capable of achieving ~72% of that theoretical maximum, which can only be achieved in a Carnot engine [56]. For rapid estimations, this translates into an ST power output that is about 50% of the combined power output of all GTs in the plant.

As the fundamental CC efficiency relationship, Eq. (15.23), and the graphical representation in Fig. 15.13 make it very clear, the cycle's heat rejection temperature is of prime importance. This temperature is dictated by the steam condenser's operation pressure, which is significantly below the atmospheric pressure. For the best performance, lowest possible steam condensation pressures, around 1.5 in. of Hg or even lower, are imperative. Achieving those low-pressure levels requires striking a delicate balance between heat rejection equipment size, cost, type, and site ambient conditions. The key heat rejection system equipment is the steam condenser. There are many types of condensers that are used to handle the heat rejection from the CC plant. Depending on the site ambient conditions, cooling medium availability, environmental regulations and customer-specific economic criteria, a suitable choice can be made. The major options are listed below.

1. Water-cooled surface condenser
   - Once-through or open-loop (utilizing a naturally available cooling water source such as lake, river, ocean)
   - Closed-loop with a natural (very rare for CC plants) or mechanical (forced or induced draft) cooling tower (CT)

2. Dry, air-cooled (also known as the "A Frame") condenser
3. Air-cooled wet surface (hybrid) or "plume abatement" condenser
4. Direct contact condenser with dry CT (Heller) system

In general, water-cooled systems, in particular open-loop systems near a relatively cold natural source of cooling water (e.g., in coastal locations in the northern hemisphere), offer the best performance, i.e., the lowest condenser pressure. How low in condenser pressure one can go is essentially a question of plant economics. Recently, permitting requirements in conjunction with environmental considerations and water scarcity in many geographic locations render water-cooled heat rejection systems infeasible. Significant size and cost of "dry" or air-cooled systems preclude the optimal condenser pressures and optimistic performance projections displayed in Fig. 15.16.

The key to affordable and sustainable large-scale electric power generation is economies of scale that can be achieved by ever-larger prime movers (gas and steam turbines of 300+ MW) and plant blocks. Modern CC plants include one or more GTs with a single ST; either in a "multi-shaft" or "single-shaft" configuration (e.g., see Figs. 15.18 and Figure 15.19). The most common multi-shaft block is 2×1 (i.e., 2 GTs and 1 ST) with power ratings of 600–900 MW. A few larger plants in 3×1 or 4×1 configuration or in multiple blocks of 2×1 are also available (e.g., see Fig. 15.18). Single-shaft (i.e., 1×1) plants with power ratings of 300–500 MW per "block" can also be combined into very large generating stations via multiple blocks. For a representative selection of modern CC power plant configuration options and performances, the reader is referred to the white papers listed in [64–68].

Even better economies of scale are achieved via the "reference plant" approach, in which OEMs develop pre-engineered modules that can be shipped and installed anywhere in the world with minimal customization to accommodate different site and customer requirements. This ensures that natural gas burning GT-CC power plants are not only the most efficient means of generating electric power available today, but also the most cost-effective (e.g., at a turnkey capital cost of $600–1,000/kW and cost of electricity of a few cents per kWh)) and fastest to build (e.g., less than 24 months of construction time). On top of all that, GTs with modern "dry low NO_x" combustors are also the cleanest fossil fuel burning technology in terms of emissions. This aspect will be explored in detail in the following section.

Cogeneration

Discussion thus far has focused on production of electricity from natural gas. When electricity is the sole product from the thermal cycle the heat rejected to ambient is termed "waste heat" because it is no longer economically useful for generation of additional power. In the larger context of a modern industrial society one finds that low temperature heat of the quality least useful for power generation has many

Fig. 15.18 Illustration of a 2×207FA (two Frame-7 60-Hz GTs with single ST) NG CC power plant. From *left* to *right*, for each GT-HRSG "block" one can see the GT inlet air filter housing and duct (on top of the GT enclosure), HRSG with drums on the top, and the stack. Two STs are located to the right of the GT-HRSG blocks (cross-over pipe and down-flow LP section are clearly visible). Note the elevation of the ST structure to accommodate the steam condenser. Partially visible to the right is the multicell mechanical cooling tower. In the lower right corner are two distillate oil (GT backup fuel) tanks (Courtesy: GE Energy)

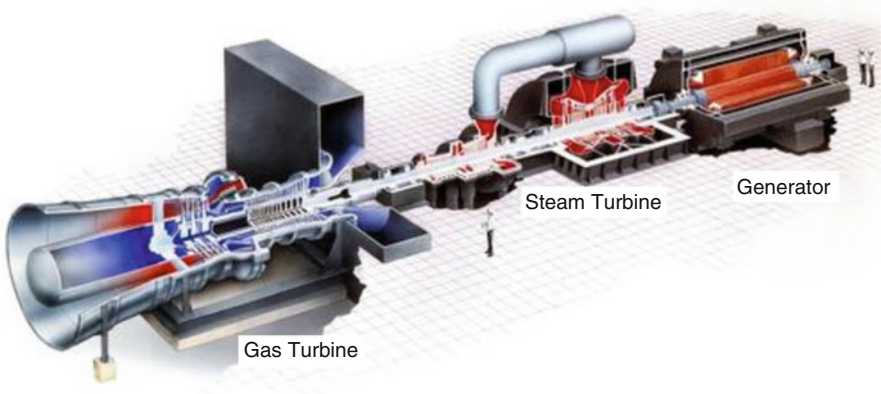

Fig. 15.19 A single-shaft combined cycle train (Courtesy: GE Energy)

economically important uses. It is thus common in industrial and urban settings to integrate a power plant with another process such that heat energy for that process is provided in whole or in part by the power cycle after the highest quality fuel energy

Table 15.5 A sampling of natural gas Fired cogeneration opportunities [71]

Industrial	
Paper and board manufacture	Pharmaceuticals and fine chemicals
Ceramics	Brewing, distilling, and malting
Textile processing	Food processing
Oil refineries	Minerals processing
Timber processing and paper	Horticulture and glasshouses
Buildings	
Hotels	District heating and cooling
Airports	Hospitals
Supermarkets and large stores	College campuses and schools
Individual houses	Office buildings

has produced some useful work. Such installations are termed cogeneration systems or Combined Heat and Power (CHP) systems and can be very efficient from an environmental and fuel use perspective. Table 15.5 provides a sampling of cogeneration opportunities with a synergistic combination of heat and power needs.

In the ideal case, the heat energy available from the prime mover (engine or thermal cycle) will always match the needs of the customer process. In practice, this is challenging since many process heat demands are variable (such as building or district heating). The electrical loads can also be out of phase with process heat demands (e.g., an electric grid with high but unsteady wind or solar renewable power contributions). These variations in electrical load vs. process heat loads can be accommodated with appropriate system design and operating strategies. A variety of cogeneration plant options are available between the extremes of a non-cogeneration facility, e.g., fired heater or boiler, with no power generation at all (e.g., a home heating system capturing the heat content of the fuel but wasting its potential to do work [69]) and the aforementioned power generation combined cycle with no process heat demand, which has accordingly been optimized for production of electricity.

Primary considerations in cogeneration system design are the size of the plant, the relative need for heat vs. electrical power, and the electricity and process heat demand variability. The following points summarize the range of system design solutions:

- Large industrial gas turbines ranging from ~20 to 300 MW electrical output are optimized for best combined cycle efficiency, and have exhaust energy of about 60% of heat input with exhaust temperatures between about 1,020°F and 1,160°F (550°C and 625°C). This class of machine is well suited to process heat demands that are large in an absolute sense but small or intermittent in relation to electrical power demand, (0% to ~30% of gas turbine heat input). This level of heat energy supply can readily be accommodated by modifying the power generation combined cycle system to include the capability to extract or divert steam from the bottoming cycle steam turbine to the process. This is a common solution for district heating which may be highly variable and seasonal.

- Aeroderivative gas turbines ranging from ~5 to 60 MW electrical output are optimized for best simple cycle efficiency, and have exhaust energy of about 55% of heat input with exhaust temperatures of about 850°F (455°C). These machines are large enough to support substantial process heat loads and are often configured in a system without a steam turbine to save cost and make a higher portion of gas turbine exhaust energy available to process. In many industrial cogeneration facilities, it is more important to match process heating demand than to meet a specific electric load. The gas turbine load is thus varied to follow process energy demand independent of electric load. Any excess electricity generated is sold to the grid and any power shortfall is purchased. If the design process heat demand is high in relation to electric load, or may occasionally need to be much higher than the unfired gas turbine exhaust energy, the system will need to include a supplemental burner in the HRSG, which can be used to boost process heat export capability. A burner may also be used in combination with part load operation of the gas turbine to maintain process heat export while reducing electricity production to match its load.
- A micro gas turbine ranging from ~0.03 to 0.3 MW electrical output may be selected if the heat load and/or electric load is small. Micro turbines typically employ uncooled regenerative cycles for best simple cycle efficiency, have exhaust energy of about 75% of heat input, and exhaust temperature of about 530°F (275°C). These units are too small to economically justify a bottoming cycle steam turbine so that they fall into the unfired or supplementary-fired heat recovery–type system configuration.
- In the size range between micro turbines and aeroderivatives, a variety of small industrial gas turbines and other prime movers such as a spark ignition reciprocating engine, or fuel cell, may also be considered. In the range from ~10 to 150 MW, direct-fired steam Rankine systems with steam turbine extraction for process heat can also be an attractive configuration that is well suited to highly variable process heat needs. Power can be varied across a wide range with modulated fuel consumption and heat export can also be widely varied via controlled steam extraction. Efficiency at low process demand is inferior to gas turbine–based systems but fuel flexibility is generally better.

Table 15.6 shows some examples of gas turbine–based natural gas–fired cogeneration systems. These are presented to elucidate the behavior of such systems and draw conclusions regarding the role of cogeneration in promoting sustainable use of natural gas. Columns tabulate net electric power export, export heat energy to power ratio, quality of export heat expressed as a ratio of its availability to produce work (exergy), electric generation efficiency, cogeneration efficiency expressed on both an energy and exergy basis, and specific CO_2 emissions also expressed on both an energy and exergy basis. Export heat is provided as steam in all cases.

Cogeneration efficiency $\eta_{c,I}$ in Table 15.6 is the straight ratio of the sum of power (kWe) and heat (kWth) products to the fuel burned in the plant on an LHV basis. This is a commonly used (sometimes with fuel input on an HHV basis) measure, which is ultimately misleading because it does not differentiate between

the "quality" of different products. In certain cases, especially with supplementary firing, it can reach improbably high values such as 90% or more.

A more rational measure is the cogeneration efficiency per the second law of thermodynamics, $\eta_{c,II}$, which uses the exergy of the thermal product rather than its energy (i.e., enthalpy) [70]. Exergy, as discussed earlier in the present article, is a direct measure of the work generating ability of a material stream via Kelvin–Planck statement of the second law of thermodynamics. Exergy is a property of a given fluid and, as such, for two given properties (e.g., pressure and temperature), it can be calculated using a suitable equation of state such as ASME steam tables. The relationship between $\eta_{c,II}$ and $\eta_{c,I}$ is given as

$$\eta_{c,II} = \eta_{c,I} \cdot \frac{1 + \beta \cdot \theta}{1 + \theta}$$

where θ is the heat-to-power ratio of the cogeneration plant, and β is the ratio of the exergy to energy (enthalpy). Since $\beta < 1$, $\eta_{c,II} < \eta_{c,I}$ and has typically a value, which is more in line with standard power plant efficiencies. In passing note that the PURPA (*Public Utility Regulatory Policies Act*, a US federal law enacted in 1978 intended to encourage more energy-efficient and environmentally friendly commercial energy production) efficiency, which is another cogeneration plant efficiency definition, is equivalent to $\eta_{c,II}$ with $\beta = 0.5$. Even $\eta_{c,II}$ is an inflated value because β is the efficiency of a hypothetical Carnot engine that converts the thermal energy to useful shaft work.

A realistic turbine that can utilize that thermal efficiency for electric power generation would have a much lower efficiency, which is characterized by the rational efficiency, ε, which is the ratio of actual turbine power output to that of the hypothetical Carnot engine. The most common thermal energy product in cogeneration is steam. Depending on the pressure and temperature of steam, with today's state of the art in ST technology, a reasonably good estimate for ε would be around 0.7. Thus, a more realistic value for $\eta_{c,II}$ would be given as

$$\eta_{c,II} = \eta_{c,I} \cdot \frac{1 + \epsilon \cdot \beta \cdot \theta}{1 + \theta}$$

Case 1 is a micro turbine–based design with no supplemental fuel addition to exhaust heat recovery. Export energy is high in relation to power production since the engine is only 25% efficient but export heat quality is low since exhaust temperature is a modest 530°F (275°C). This low exhaust temperature also compromises the cogeneration energy efficiency in these examples because only a portion of the unfired exhaust energy is recoverable to steam.

Case 2 adds a supplemental burner fired to 1,600°F (871°C) to boost export energy substantially while also improving its quality. Fuel heat energy is now fully utilized to provide power and process heat (93% cogeneration efficiency, energy

Table 15.6 Typical heat-to-power ratios and efficiencies for GT-based CHP systems

								Engine+Burner CO_2 Emissions	
		Net power (MWe)	θ	β	$\eta_{el.}$ (%)	$\eta_{c,I}$ (%)	$\eta_{c,II}$ (%)	*A*	*B*
1.	Unfired micro GT	0.1	1.74:1	0.29	25.4	69.6	38.3	284.7	516.9
2.	Supplementary fired micro GT	0.1	10.0:1	0.44	8.6	93.0	46.6	212.9	418.3
3.	Unfired aeroderivative GT	40	1.13:1	0.41	41.2	87.8	60.4	225.4	327.7
4.	Supplementary fired Aeroderivative GT	40	2.63:1	0.44	26.3	93.0	56.6	212.9	349.6
5.	Unfired industrial GT	100	1.50:1	0.45	35.6	89.0	59.5	222.5	332.8
6.	Supplementary fired Industrial GT	100	2.84:1	0.44	24.8	93.0	55.7	212.9	355.4
7.	Gas turbine combined cycle (unfired, industrial GT)	100	0.1:1	0.29	54.3	59.7	55.9	331.8	354.4
			0.5:1	0.34	49.1	73.6	57.4	269	344.7
			1.0:1	0.38	42.4	84.9	58.7	233.3	337.2
8.	Gas turbine combined cycle (industrial GT with supplementary firing)	100	1.5:1	0.44	35.2	88.0	58.5	225.1	338.8
			2.0:1	0.44	31.6	93.0	59.4	212.9	333.2

θ is heat to power ratio in kWth/kWe
β is heat quality, which is the ratio of export exergy to export energy
$\eta_{el.}$ is electric generation efficiency
$\eta_{c,I}$ is first law cogeneration efficiency (energy-to-fuel input)
$\eta_{c,II}$ is second law cogeneration efficiency (exergy-to-fuel input)
Emissions are in g/kWh of energy (*A*) and exergy (*B*)

basis), but the performance is still modest on an exergy basis since the engine is inefficient. Note also that specific CO_2 emissions (exergy basis) improved because the incremental efficiency due to increased and improved heat export is better than the electrical efficiency of the gas turbine.

Cases 3 and *4* show the corresponding story for a 40 MW aeroderivative gas turbine while *cases 5* and *6* present a 100 MW industrial gas turbine scenario. These gas turbines both improve exergetic performance over the micro turbine cases but when supplemental firing is added the cogeneration efficiency and specific CO_2 emissions (exergy basis) both degrade. The more efficient aeroderivative has slightly higher system performance but lower process heat export capability vs. the industrial gas turbine.

Case 7 shows the 100 MW industrial gas turbine in a combined cycle configuration with increasing steam extraction to process. Electric generation efficiency falls off as more energy is diverted to process while cogeneration efficiencies improve. *Case 8* begins where case 7 left off with power output maintained as supplemental firing is increased. By the time 1,600°F (871°C) supplemental firing temperature is reached the export heat energy has approximately doubled. As supplementary firing increases the specific CO_2 emissions (exergy basis) stays approximately constant.

Note that the supplementary-fired scenarios presented here stop at 1,600°F (871°C) consistent with uncooled metal ductwork. Firing temperature can be pushed further by application of refractory or water-cooled walls until the excess oxygen is nearly expended; or increased even further if supplemental air is also added. High supplementary firing may be required for some applications but is less desirable from a resource conservation perspective than a design with little (or no) supplementary firing.

The following general conclusions can be drawn from this sampling:

1. Cogeneration efficiency should be expressed on an exergy basis to promote the most sustainable use of fossil fuels. Direct use of fuel for low-quality end uses represents a large waste of the thermodynamic potential inherent in the fuel. Cogeneration efficiency as commonly expressed in relation to export energy gives the false impression that supplementary firing improves the environmental (CO_2) and resource (natural gas) utilization performance.
2. Cogeneration system configuration will be a function of the quality and quantity of heat energy required, its variability, and the relative heat and power needs. A wide range of applications can be served by appropriate system design.
3. Gas turbine–based systems are most efficient when not supplementary fired while gas turbine combined cycle cogeneration systems maintain high cogeneration exergetic efficiency even with supplemental firing. This is because fuel energy can be recovered to power all the way down to the temperature level required by the process user.

Figure 15.20 shows cogeneration's contribution to electricity production in European Union countries.

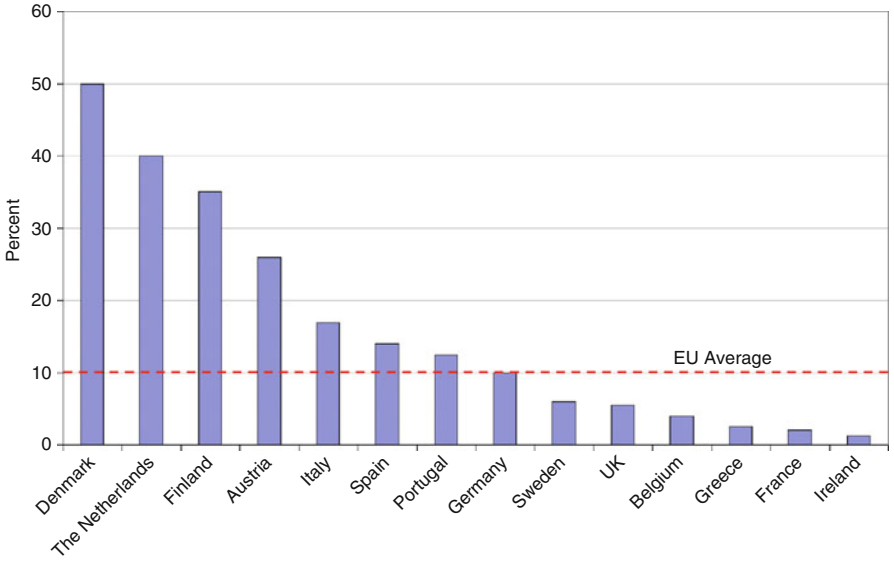

Fig. 15.20 Cogeneration as a share of national power production (1999) (Source: European Association for the Promotion of Cogeneration [71])

The higher penetration seen in four of these countries is attributed to a combination of favorable economics and supportive government energy policy [71]. In the USA, approximately 4% of electricity production currently comes from cogeneration facilities of which 71% are fueled by natural gas (e.g., see Table 8.2c in [72]).

How far could cogeneration penetrate in the USA and what benefits would accrue? Just as it is possible to look at the utilization rate of renewable energy sources such as wind, hydro, and solar in relation to the size and distribution of these resources, the thermal power plant heat available for low-temperature end users can be quantified to estimate the potential for increased cogeneration and hence its potential to offset other fuel use and emissions.

The annual US thermal power generation totaled 3.7 trillion kWh in 2008 [72]. Factoring in the mix of natural gas–fired systems, nuclear, and direct-fired (mostly coal) plants and their respective thermal efficiencies allow estimation of heat resources available for cogeneration. Table 15.7 shows an estimated breakdown of heat rejection from thermal power plants in the USA.

While cogeneration with direct-fired or nuclear-fueled Rankine systems is certainly possible, the sheer size of these plants makes it difficult to economically match them to end users that themselves are large enough to benefit from the full heat energy available. For this reason, cogeneration systems tend to be relatively small in terms of electrical output, which in turn aligns well with the NG-fired gas turbine and gas turbine combined cycle. Natural gas accounts for 883 billion kWh

Table 15.7 Annual US thermal energy available supply and rejection, 2008 [72, 73]

			Natural gas				
	Coal	Petroleum	Combined cycle	Simple cycle	Cogeneration	Nuclear	Total
Electricity generation (Billion kWh)	1,986	46.2	562	122	200	806	3,721
Heat rate (Btu/kWh, HHV)	9,884	9,884	7,598	11,526	11,156	10,488	
Heat input (trillion Btu)	19,628	457	4,268	1,402	2,227	8,456	36,062
Approximate heat rejection to ambient or process (trillion Btu)	10,889	254	1,408	847	1,159	5,451	19,730
Heat rejection beta (β)	0.20	0.20	0.20	0.44	0.44	0.20	

or 23.7% of total electricity generation [72, 73]; 199.7 billion kWh or 22.6% of which comes from cogeneration facilities (e.g., see Table 2.1 in [73]). Taking the data in Table 15.6 for cases 5 and 6 as a typical system configuration, it is possible to estimate the current fuel savings from natural gas–fired cogeneration as follows.

Natural Gas–Fired Cogeneration (GT+Supplemental Firing)

1	Electricity generation (billion kWh, 2008)	200
2	Combined cycle heat rate (Btu/kWh, HHV)	8,305
3	GT heat input (trillion Btu, 2008)	1,658
4	System heat rate (Btu/kWh, HHV)	11,156
5	Burner supplemental heat input (trillion Btu, 2008)	569
6	System heat input (trillion Btu, 2008)	2,228
7	Heat export to process (trillion Btu, 2008)	1,159
8	Equivalent heat input to meet process (trillion Btu, 2008)	1,302
	Cogeneration natural gas savings (trillion Btu, 2008) (Line 8 minus Line 5)	733

The fuel savings from application of cogeneration represents ~24.8% reduction in fuel burn vs. making the power with a gas turbine combined cycle and supplying the heat independently with a fired boiler. CO_2 emissions reductions follow the fuel saving directly if the fuel saving is booked as natural gas. If booked at the current fuel mix for US electricity production, the CO_2 savings are higher by about 33% or higher by 75% if booked as reduced coal fired generation. Looking at the heat

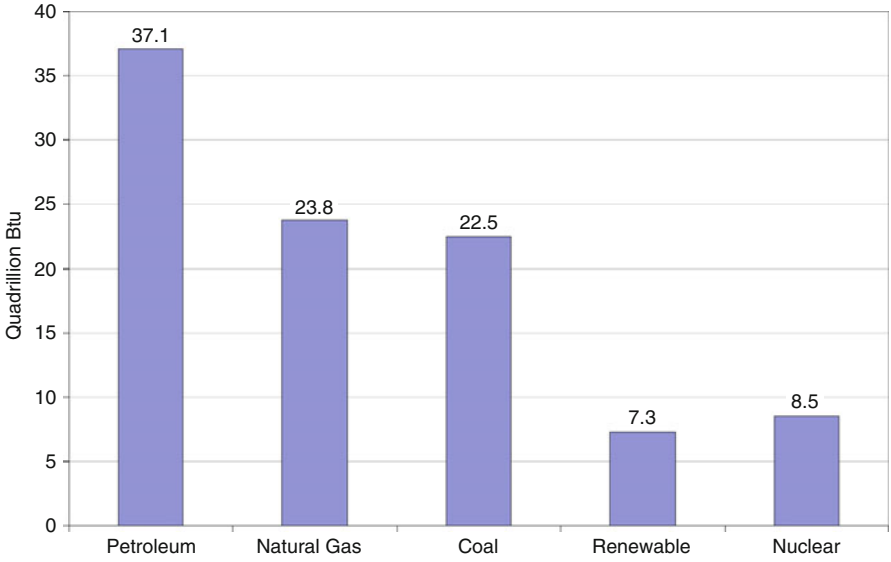

Fig. 15.21 Primary energy production by source, 2008. Total primary consumption is 99.3 quadrillion Btu. Renewable energy sources are hydroelectric power, geothermal, solar/photovoltaic, wind, and biomass. "Petroleum" does not include the fuel ethanol portion of motor gasoline – fuel ethanol is included in "Renewable Energy." "Natural Gas" excludes supplemental gaseous fuels. "Coal" includes less than 0.1 quadrillion Btu of coal coke net imports (Source: Energy Information Administration (EIA) [72])

rejection from natural gas–fired power generation in the USA in Table 15.7, in comparison to current heat export from natural gas-fueled cogeneration, it appears that the amount of cogeneration could perhaps be doubled without a major shift in fuel use patterns. Reaching the electricity contribution levels seen in some small European countries would likely require more distributed generation with replacement of large coal-fired power plants with more small cogeneration systems (likely gas fired) proximate to potential end users.

Turning now to the potential customers for heat energy, Fig. 15.21 shows the primary energy production by source in the USA for 2008 [72]. Fig. 15.22 shows the incremental retail electric load distributed to each sector and gives a breakdown between residential and commercial sectors. The natural gas contribution to the residential and commercial sectors is 8.2 trillion Btu [72]. Assuming that its primary use is for space heating, it can be seen that it far exceeds the available waste heat from gas-fired power plants tabulated in Table 15.7. It is difficult to make the case that small (micro) cogeneration systems could be aligned to the heat and power needs at the individual house level, though work on fuel cell systems for this purpose is active. The commercial sector and high-density residential (e.g., apartment complex) does offer real potential for expansion. In either case, the performance of the cogeneration system needs to be high enough to improve on the fuel use and environmental performance of an efficient utility scale power plant in combination with direct use of natural gas for heating.

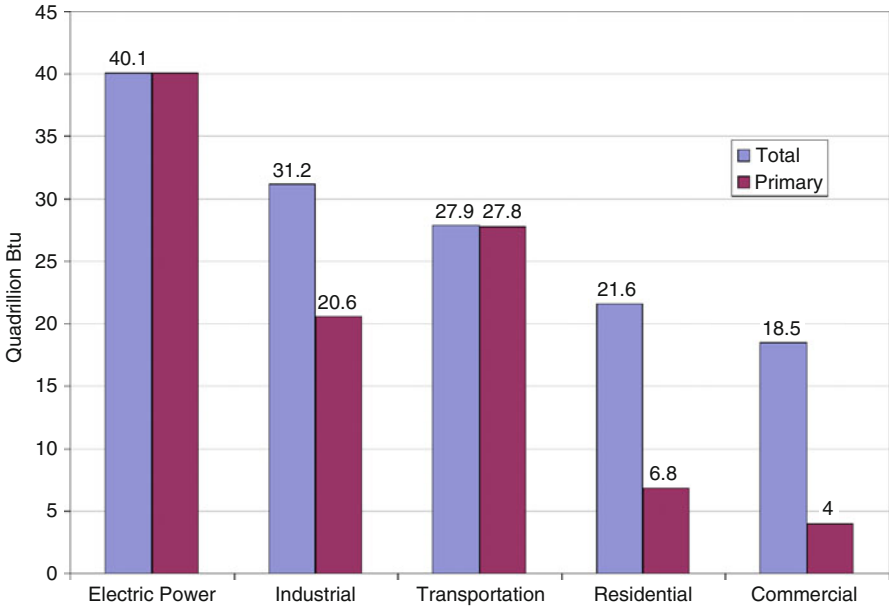

Fig. 15.22 Primary and total consumption by sector, 2008. See Fig. 15.21 for a breakdown of sources (Source: Energy Information Administration (EIA) [72])

Combustion and Emissions

There are different types of GT combustors that have been used at one time or another by different OEMs in their products:

1. Silo (obsolete now, once used by Siemens and former ABB)
2. Annular (aero-derivatives such as GE LM6000)
3. Can or tubular (heavy-duty industrial GTs by Siemens, GE)

In the following discussion a parameter will appear frequently, i.e., the *equivalence ratio*, ϕ, which is the ratio of the actual fuel-air ratio, *f*, to the *stoichiometric* fuel air ratio. The latter is the theoretical value requisite for complete combustion. Thus,

$$\phi = f_{\text{act}}/f_{\text{st}}$$

When the equivalence ratio is equal to 1.0, the flame temperature is the highest and the chemical reactions are the fastest. Thus,

1. If ϕ is less than 1.0, the mixture that reacts is referred to as "lean" or "fuel lean."
2. If ϕ is greater than 1.0, the mixture that reacts is referred to as "rich" or "fuel rich."

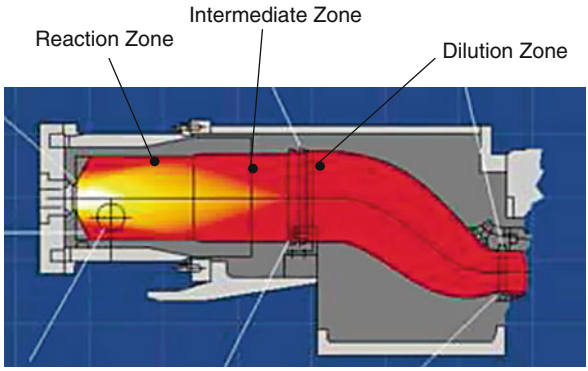

Fig. 15.23 Single-Nozzle Diffusion (SND) Combustor

In either lean or rich combustion, flame temperature is lower and chemical reaction is slower than their stoichiometric counterparts.

The can-type combustor can be divided into three zones (see Fig. 15.23):

Primary Zone (PZ): This is the combustor *reaction* or flame zone where fuel is injected and mixes with air (about 15–20% of the compressor discharge air is introduced). In order to cap the combustor exit temperatures at a level, which downstream turbine HGP components can tolerate, the requisite value of ϕ is typically 0.4–0.5, which is too lean for stable and efficient burning. This is why only a portion of the combustion air is introduced into the primary zone. High-temperature rapid combustion takes place in the PZ. The design of this part of the combustor must facilitate highly turbulent and recirculating flow pattern to anchor the flame at the exit of the fuel injector nozzle. This is critical because of the high-speed of the air stream, even at a fraction of its full value, which is an order of magnitude higher than the turbulent flame speed at which the flame propagates into the fuel-air mixture.

Secondary Zone (SZ): This is the *intermediate* zone where a portion of the remaining combustion air ($\sim$30% of the total) is introduced in the mid-section of the can through holes or cooling slots in the combustor liner. The hot combustion gas from the PZ gets thermally soaked and the combustion is completed. The air that flows between the liner and flow sleeve and enters the can forms a film to cool the liner wall.

Dilution Zone: This is where the remaining air enters the can through the metering holes and cools the gases to the desired temperature. A design to promote turbulence and thorough mixing of hot and cold streams is essential to ensure a homogeneous temperature distribution and prevent hot streaks.

A successful combustor design should satisfy the following criteria:

1. Efficient and stable operation, which comprises the following characteristics
2. Complete combustion at or near stoichiometric flame temperature

3. Flame stability and reliability at high turndown
   (a) Ignition
   (b) Crossfire (propagation of flame from fired chambers with spark plugs to the unfired chambers via tubes interconnecting the annular combustion chambers or cans)
   (c) Lean blowout
4. Operational stability and reliability at high turndown
   (a) Dynamics (noise), i.e., large-amplitude pressure oscillations in combustion chamber, driven by heat release oscillations; also known as combustion "humming." These oscillations are destructive to engine hardware.
   (b) Pattern factor, which is a measure of the temperature distribution at the combustor exit defined as $PF = \frac{T_{\text{peak}} - T_{\text{mean}}}{T_{\text{mean}} - T_{\text{inlet}}}$
   (c) Pressure drop
5. Low emissions in compliance with regulatory laws

Achieving these goals simultaneously is very difficult due to the counter-acting impacts of design parameters on each criterion. The design history of the GE heavy-duty industrial gas turbine combustors can be found in Ref. [74]. The design evolution can be summarized in three major designs:

1. Single-nozzle diffusion (SND) combustor
2. Multi-nozzle, quiet combustor (MNQC)
3. DLN or Dry-Low-NO_x combustor

The design evolution was primarily driven by the desire to satisfy the increasingly stringent emission control requirements with improved efficiency via higher combustion and turbine inlet temperatures (TIT). In order to clarify this, one must be familiar with the chemical mechanisms of NO_x production, which is one of the most critical pollutants present in GT exhaust gas. Principal pollutants emitted by a GT are as follows [75]:

1. Oxides of nitrogen (NO_x), which are toxic, contribute to chemical smog and lead to depletion of ozone in stratosphere
2. Oxides of sulfur (SO_x), which are toxic and corrosive
3. Carbon dioxide (CO_2), which contributes to greenhouse effect and global warming
4. Carbon monoxide (CO), which is toxic and asphyxiating
5. Unburned hydrocarbons (UHC), including volatile organic compounds (VOC), which contribute to urban smog
6. Particulate matter (PM), which is suspected to cause respiratory diseases

Detailed information on GT emissions and control can be found in Ref. [76]. Some pollutants, i.e., UHC, PM, and SO_x, are generally of no concern for GTs burning gaseous fuel with the exception of coal-gasification SG, which leads to conversion of fuel-contained sulfur to SO_x. (Note, however, that in some cases contamination

of fuel in the pipeline, e.g., rust particles, can be a problem for HGP components). In any event, currently there is no available GT combustion technology to prevent or control SO_x emissions. Similarly, CO_2 is a direct product of the complete combustion process and cannot be controlled or reduced within the GT control volume (except, of course, increasing the thermal efficiency of the GT, which will reduce the amount of fuel consumed and CO_2 generated for a given power output). Precombustion or postcombustion capture and storage of carbon dioxide, known as carbon capture and storage (CCS), is currently a hot topic of research and development.

A key pollutant emitted by the GT is NO_x. There are two major sources of NO_x:

1. Atmospheric N_2 in post-flame gases, which leads to formation of NO and NO_2 via three principle mechanisms:
   (a) Thermal NO (extended Zel'dovich mechanism)
   (b) Nitrous oxide mechanism
   (c) Prompt NO mechanism
2. Organically bounded nitrogen in fuel or fuel-bound nitrogen (FBN)

The dominant NO_x formation mechanism is the thermal or Zel'dovich mechanism. Although not a significant source of NO_x for NG, FBN in low-quality liquid fuels and LCV gases with hot-gas clean-up (via ammonia) can be high enough to merit attention. NO_x (and CO) formation is a function of three primary parameters:

1. Residence time in the combustion zone
2. Chemical reaction rate
3. Mixing rate

These three reaction parameters can be related to the turbine operating conditions and combustor size [75]. In particular,

$$\text{Residence time} \propto \frac{p \cdot V_c}{\dot{m} \cdot T_{pz}} \tag{15.27}$$

$$\text{Reaction time} \propto p^n \cdot \exp(kT_{st}) \tag{15.28}$$

where

- T_{st} is stoichiometric flame temperature (or, equivalently, f or ϕ or firing temperature)
- T_{pz} is the average gas temperature in the reaction or primary zone
- V_c is combustion volume
- p is combustion pressure (raised to a power of n)
- $\dot{m}$ is the combustor mass flow rate

Therefore, NO_x production rate can be expressed in an empirical formula that can be written as

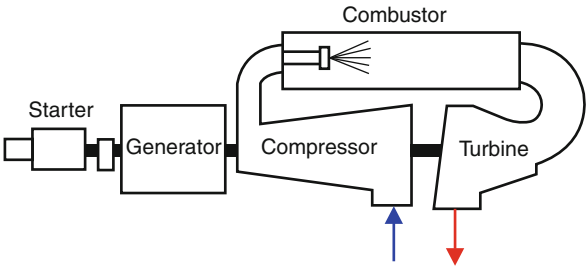

Fig. 15.24 Effect of pressure and stoichiometric flame temperature on NO_x

$$NO_x \propto \frac{V_c}{\dot{m} \cdot T_{pz}} \cdot p^{1+n} \cdot \exp(k \cdot T_{st}) \tag{15.29}$$

The relationship between NO_x production and key parameters per Eq. (15.29) is shown qualitatively in Fig. 15.24. In general, NO_x values are reported in parts per million (ppm) on a dry basis (usually expressed as ppmvd) and corrected to 15% O_2 in combustion air. It is extremely important to make sure that the basis of the reported number is clearly defined; otherwise comparisons of data from different sources can be misleading. The expression for correction is as follows:

$$[NO_x]_{15\%O_2} = \frac{[NO_x] \cdot 5.9}{(20.9 - O_{2,meas})} \tag{15.30}$$

The trends in Fig. 15.24 show that the impact of pressure on NO_x formation is stronger at high flame temperatures near the stoichiometric value (i.e., $\phi \sim 1.0$) and negligible at leaner mixtures with lower flame temperatures. Consequently, effective control of the NO_x production in the combustion process is a matter of reducing the flame temperature. There are essentially three ways to accomplish this:

1. Design a primary (reaction) zone with leaner fuel-air mixture
2. Injection of a diluent, i.e., water or steam, into the primary zone of the combustor to act as a "heat sink" and reduce the flame temperature
3. Staged combustion with two distinct reaction zones, which lead to the modern "lean-premixed" designs, which is referred to as *Dry-Low-NO_x* (or *DLN*).

The dramatic impact of reducing ϕ, i.e., leaning out the PZ, on flame temperature and NO_x production can be seen in Fig. 15.25. Leaner fuel-air mixtures lead to lower-value flame and gas temperatures and favorably impact the NO_x production rate via shorter residence and reaction times.

Unfortunately, things get complicated rapidly. For starters, the full operating range of an industrial GT combustor requires significant turn-down ratios, e.g., 40-to-1 in fuel flow, 30-to-1 in air flow, and 5-to-1 in fuel-air ratio. Obviously, the combustor design must ensure stable and efficient combustion across the entire operating range. The early single-nozzle (diffusion flame) combustors, with direct injection of fuel and air into the PZ, were designed for combustion at or near

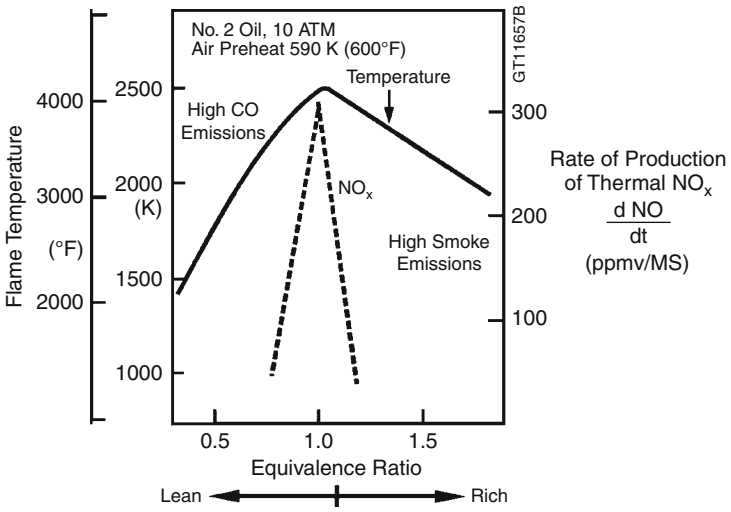

Fig. 15.25 Thermal NO_x production rate (Source: GE Energy [74])

stoichiometric conditions. For a combustor designed for optimal full load operation at $\phi \sim 1$, combustion at lower loads is bound to be very lean. Thus, further leaning out of the PZ for NO_x reduction is a very limited knob. In fact, initial efforts to reduce NO_x via leaning out reaction zone of an SND combustor did not achieve more than 20% reduction [77].

When it became clear that meeting increasingly stringent pollution-control regulations via leaner reaction zones in SND combustors, other methods to reduce flame temperatures were investigated. Injection of water or steam into the PZ to create a "heat sink" for temperature reduction proved successful. Starting in 1979, when regulations required that NO_x emissions be limited to 75 ppmvd, SND combustors with water or steam injection have been successfully used to meet or exceed these requirements successfully [74]. However, SND combustors that use water and steam injection are limited in their ability to reduce NO_x levels below 42 ppmvd on gas fuel (65 ppmvd on oil fuel). The main reason is the practical limit to the amount of diluent injection into the reaction zone before the increase in dynamic pressure oscillations (i.e., noise) start imposing unacceptable penalties in terms of reduced hardware life and increased maintenance frequencies. High levels of water injection excited discrete dynamic pressure tones within the combustor. Frequencies within the range of the hardware's natural frequency resulted in combustor damage. In terms of dynamic pressure response, steam is a better diluent than water, although a larger mass flow rate is needed. Significant reduction in NO_x production is achievable via steam injection, e.g., $\sim$60% at a steam-to-fuel ratio of unity [77, 78].

The other significant drawback on water or steam injection for NO_x abatement is the overall simple or combined cycle performance penalty. Even though the turbine

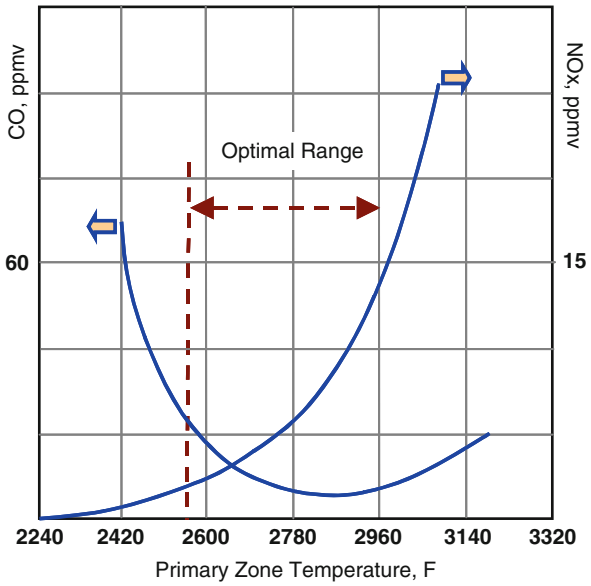

Fig. 15.26 Influence of PZ temperature on CO and NO_x [75]

output increases via increased mass flow, the associated increase in fuel consumption is detrimental to the heat rate. Furthermore, since the quality of injection water must be high, i.e., of boiler quality, to prevent deposits and corrosion in HGP components, additional *water treatment system* (WTS) cost for simple cycle applications must be considered. In combined cycle applications, where steam from the HRSG or ST (typically *cold reheat* steam) is extracted for injection, increased make-up flow rates and ensuing WTS size increase and water consumption are additional concerns. Even disregarding the combustion noise and life issues, it is easy to imagine that ever-increasing turbine-firing temperatures for improved cycle efficiency would drive the diluent injection flows to such levels where they would literally put the flame out. This is notwithstanding the counterproductive effect of reduced cycle efficiency via higher fuel consumption, which defeats the purpose of increasing the firing temperature in the first place.

Another limit associated with lowering the equivalence ratio and flame temperature for NO_x abatement is the increase in CO emissions. The conflicting emission benefits and harms of lowering or increasing the flame temperature can be seen in Fig. 15.26. Carbon monoxide is a measure of combustion inefficiency, which becomes more pronounced at leaner combustions. This is due to shorter residence time at leaner mixtures, which does not lend itself to complete CO burnout. Thus, the allowable temperature range for emissions control is limited to a relatively narrow band of ~400°F.

When SND combustors hit a practical limit for NO_x emissions reduction, even with diluent injection, designers responded by developing the "*multi-nozzle quiet*

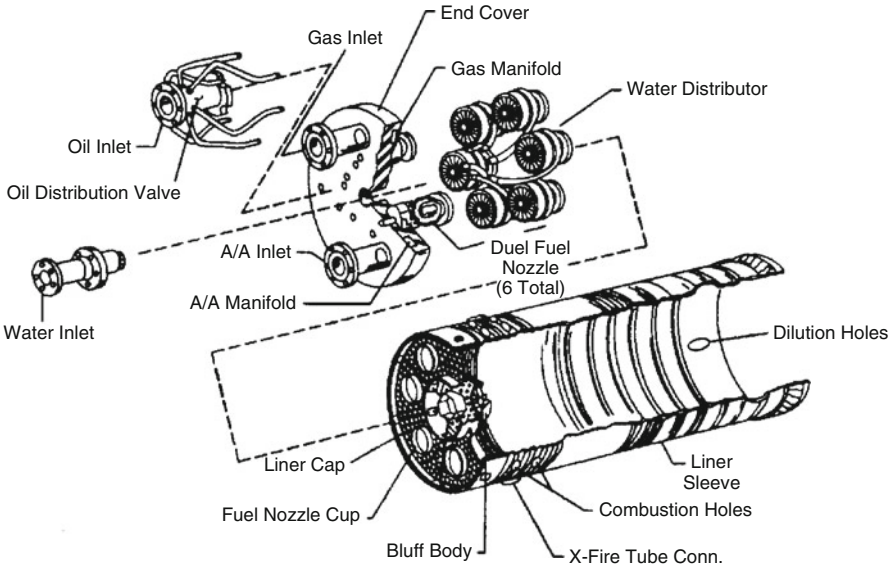

Fig. 15.27 MNQC Combustor (Source: GE Energy [79])

combustion" or MNQC system. For a detailed history of the combustor development, please consult Ref. [74]. Utilizing a multi-nozzle configuration, i.e., six nozzles located peripherally at the combustor head cap, this system eschewed the low-speed ignition and blowout problems associated with excessive leaning out of the PZ in SND systems at low loads (see Fig. 15.27). Furthermore, the MNQC system also helped with the dynamic pressure oscillation (i.e., noise) problem by maintaining a flat dynamic response at increased steam injection levels (that is the reason for the moniker "quiet"), thus enabling the design of combustion systems with higher firing temperatures and compliant NO_x emissions without the problems of increased hardware wear and reduced maintenance intervals. Since 1987, MNQC systems enabled heavy-duty GTs to meet stringent NO_x emission requirements, i.e., 25 ppmvd with gas fuels and 42 ppmvd with liquid fuels. Increase in CO and UHC emissions and combustion stability issues at high injection rates, e.g., steam-to-fuel >2, precluded further improvement with this technology [80].

Reduction in NO_x emissions to even lower levels, the need for balancing the low emissions with ever-increasing firing temperatures and the need to avoid the cycle thermal efficiency penalty associated with steam and water injection lead to the development of DLN combustors. DLN combustion system is the natural next-step in combustor development, i.e., a "staged" combustion system with lean-premixed fuel-air mixture. The primary and secondary combustion zones in the staged combustor are operated at the lowest possible ϕ at high fuel flow conditions (see Fig. 15.28). During start-up, acceleration, and low-load conditions, fuel is introduced only in the PZ with good ignition and blowout characteristics. At increasing load levels, fuel is introduced into the SZ at a fuel split to balance the CO and NO_x production at an

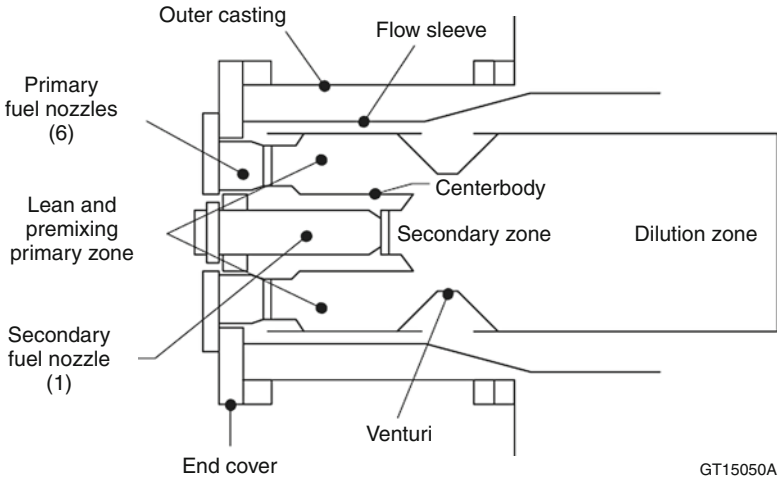

Fig. 15.28 Dry-Low-NO_x (DLN) combustor (Source: GE Energy [80])

optimal level, i.e., near the middle of the allowable range shown in Fig. 15.25. The first successful DLN system, DLN-I, that went into production incorporated a multi-nozzle system similar to that in MNQC for the PZ and a conventional, large secondary fuel nozzle for the SZ. At normal (50–100% load) operation, fuel and air are "premixed" in the PZ but ignition takes place in the SZ with the flame attached to the secondary nozzle.

DLN technology successfully balanced the requirements for low combustion noise (i.e., dynamic stability) at part-load operation and optimal equivalence ratio for minimum NO_x at acceptable CO levels. DLN achieves this balance without diluent injection (and associated efficiency penalty and cost) while satisfying the requirement for low NO_x emissions, i.e., 25 ppm or lower on gas fuels. A history of the development of DLN-I and DLN-II (for F-Class turbines with high firing temperatures of 2,400+°F) systems can be found in Ref. [74] along with a detailed description of DLN operation modes.

Basic Economics

Natural gas–fired gas turbines and GTCC power plants are the most economic choices for fossil fuel–based electric power generation. This is clearly represented by the data in Table 15.8. The data in the table reflects 2004 prices. The numbers and the relative position of NG-fired plants should be expected to show a certain variation as a function of changing economic climate (i.e., inflation, demand for generating capacity, absolute and relative fuel prices, labor shortage, raw material prices, etc.) of which the recent worldwide depression that started in the last quarter

of 2008 is a very good example. Nevertheless, a dramatic shift in the economic advantages of the CC plants vis-à-vis other nonrenewable large central stations or renewable options (i.e., wind, solar, etc.), which cost nearly ten times per kW capacity and available only in small sizes amenable to distributed power generation, should not be expected near term. A very brief introduction to the key aspects of the CC plant economics, i.e., plant capital (turnkey) cost or price and the cost of generating 1 kWh of electric power, is therefore quite useful.

Turnkey combined cycle plant price levels from 2009 Gas Turbine World (GTW) Handbook are shown in Fig. 15.29. Note that listed GTW prices are in 2009 US dollars for a basic natural gas–fired combined cycle with gas turbine generator, unfired multi-pressure heat recovery boiler with no bypass stack, condensing multi-pressure steam turbine generator, step-up transformer, water-cooled heat rejection, standard controls, starting system, and plant auxiliaries. Obviously, depending on the scope of equipment, site-specific requirements, geographic location, and competitive market conditions these prices will vary considerably. Also excluded from the prices in GTW are the indirect costs and other commercial outlays. For a more realistic price level, the data in Fig. 15.29 reflects an adder of about 60% to the listed price, which is based on the assumption that the prices in GTW reflect only 75% of the direct costs, which are 85% of the total installed cost (see Fig. 15.30 and Table 15.9 below).

The data plotted in Fig. 15.29 can be summarized by the power law

$$k = 2,890 \cdot P^{-0.2012} \tag{15.31}$$

where k is the specific price ($/kW) and P is the net plant output in MW (with R^2=0.994). In general, an exponent of 0.2–0.3 is adequate to estimate the capital cost of a CC plant from a known data point (i.e., price and net output). There are several methods and tools to calculate CC power plant cost (from a plant owner's perspective), which are used within OEMs and A&E firms and not available for public consumption. Well-established cost-estimating techniques, especially those that are adopted by the CPI, are readily available in textbooks and scholarly articles. For a discussion of those and the underlying details, the reader is referred to Reference [81]. Another valuable source is Reference [82].

Calculation of the final cost of the CC plant requires consideration of many elements. In fact, the total cost of GT and ST generators and the HRSG, which are the major equipments in the CC power plant, comprises about 50% of the total plant cost. A typical distribution is shown in Fig. 15.30 from Ref. [83]. In addition to these "direct" costs, there are "indirect costs" that can contribute anywhere between 15% and 30% to the final cost of the CC power plant. As an example, consider the representative breakdown in Table 15.9.

The presented data should suffice to give an idea about the scope of the CC plant capital cost and its importance from a design engineer's perspective. All design performance calculations should be evaluated with an eye to the final plant cost. That final plant cost is the money, i.e., the plant "price," that is going to come out of

Table 15.8 Cost and performance of nonrenewable electric power generation plants

		Economic life	Lead time		Efficiency		Fuel cost	Fixed	Variable
	Capital cost per kW	years		Load factor %	%	% (CHP)	$/MMBtu	$/kW-year	$/MWh
NG-fired GT	$350–500	30	1.5	5–50	38			9–12	4
NG-fired GTCC	$550–900	30	2	60–85	55		4–5	10–15	2
NG-fired GTCC with CHP	$600–700	30	2	50–85	40–55	79–84		10–15	2
US SCPC	$1,300–1,800	30	4	60–85	35–42			20–25	3
US IGCC	$1,700–2,100	30	4	60–85	39–42		0.75–1.50	30–35	2
Nuclear	$2,000–3,000	40	6	85–92	33		0.5	60–70	1.5

Source: Cambridge Energy Research Associates, MA, USA

Load factor specifies the percent of (equivalent) hours in a year (8,760 h) during which the plant runs at its nominal base load. The data reflects the 2004 prices

CHP Combined Heat and Power (also known as Cogeneration), *SCPC* Supercritical Pulverized Coal, *IGCC* Integrated (Coal) Gasification Combined Cycle

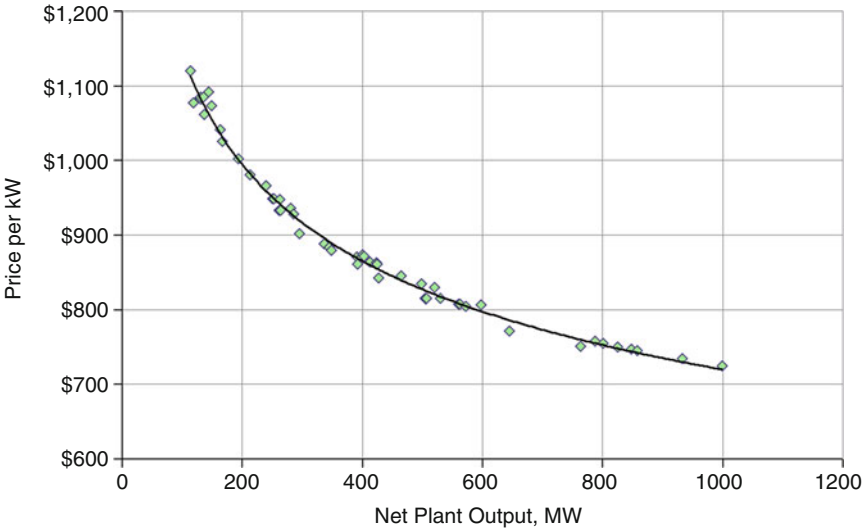

Fig. 15.29 Turnkey CC plant prices from Gas Turbine World 2009 Handbook. An adder of about 60% is applied to the listed price, which is budgetary turnkey equipment package price, to account for items not covered (see Fig. 15.30 and Table 15.9 below). Provided for reference only

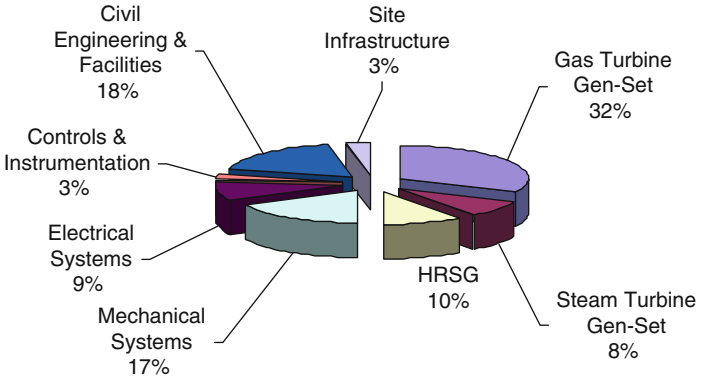

Fig. 15.30 Direct cost breakdown for a typical 400 MW CCPP (Source: Reference [83], pp 16)

the plant owner's pockets or his credit sources and thus directly impact the generation cost of 1 kWh of electricity.

Probably the most critical customer criterion for choosing an electric power generation product is the life cycle cost of ownership. The metric that is used to quantify this cost is the unit (per kWh) cost of generating electricity. Cost of electricity (COE), in its most commonly used form, is a simple formula that

Table 15.9 Typical CC capital cost breakdown between direct and indirect costs. From Energy Issues (World Bank), No. 20 June 1999, which is based on a 350/700 MW CC Plant with a Siemens-Westinghouse V94.3A (now SGT5-4000 F) GT

Integrated services (Indirect costs)	Contribution to total CC cost (%)
Project management and subcontracting	4
Plant and project engineering//software	2
Plant construction, commissioning, and training	8
Transport and insurance	1
Direct costs	**Contribution to total CC cost (%)**
Civil works	15
Gas and steam turbine generators	32
Boiler island	11
BOP	16
Electrical systems	7
Instruments and control	4

combines a power generation system's cost (capital and operating) and thermal performance into a single figure of merit that enables comparison of different systems. It is given as:

$$\mathrm{COE} = \frac{\beta \cdot k}{H} + \frac{L \cdot f}{\eta} + \mathrm{OM} \tag{15.32}$$

where β = Capital charge factor k = Total plant specific cost in $/kW H = Annual operating hours f = First-year fuel cost in $/MMBtu(HHV) L = Levelization factor η = Net efficiency of the CC plant OM = Operating & maintenance costs, $/kWh.

The first term on the right-hand side of Eq. (15.32) represents the carrying charges, the second term is the cost of fuel, and the last term is the cost of maintaining and operating the plant. Fuel cost and operation and maintenance (O&M) costs are the variable components of the COE whereas carrying charge is the fixed component. COE is typically calculated over the economic lifetime of the plant (typically 30 years).

Levelization factor, L, converts the fuel cost that usually escalates over the plant's economic life due to market conditions and inflation into average annual (constant) values. The formula for L can be found in any financial reference and is a function of discount, escalation, and inflation rates.

The fixed charge rate, β, represents the plant's financial and tax situation and is a function of the economic life of the power plant, debt–equity ratio used in financing the plant, debt and equity rates, corporate tax rate and tax credits, book depreciation, property tax, and insurance. Various methods are available for calculating β, which can be found in plant economic studies. Typical values of β are 16–18% for *Independent Power Producers* (IPPs) and 12–13% for government-owned utilities, depending on the interest and taxation rates.

If the new and clean performance conditions are used within the calculations, the cost of generation as given by the COE formula should be treated as a figure of merit rather than an accurate assessment of the "real" generating cost. Important drivers – such as seasonal variations in ambient conditions, part load operation, recoverable and unrecoverable component deterioration, uncertainty in fuel prices, start-up and shutdown, and unforeseen events – are not considered. Nevertheless, levelized COE is an important metric that provides insight to performance-cost trade-offs for OEMs (system design) as well as customers (system selection).

The exact distribution of the cost of generating 1 kWh of electric energy varies depending on the financial assumptions. Typically, about two-thirds of the COE for an NG-fired, medium-loaded (~6,000 h/year) modern 3PRH CC plant with an F-Class gas turbine is the fuel cost. About one fourth of the COE is the capital cost. The distribution is markedly different (actually, nearly exactly the opposite of NGCC) for the IGCC plant with very high capital expenditure ($2,000/kW or even higher) utilizing a cheaper fuel, coal ($1–2).

Future Directions

At the time of writing of this article, natural gas accounts for about 22% of US electricity generation. The share of natural gas in electricity generation in OECD member countries in Europe is about the same. The share of natural gas is expected to increase in the future to the tune of 25% of total world electricity generation by 2030 [2]. However, recent developments suggest that this projection might in fact be a low estimate. One reason is the new drilling technologies that made extraction of natural gas from shale rocks feasible. The technique is called *hydraulic fracturing* and involves injection of high-pressure water into rock formations to destroy them and enable the trapped gas to be released to the surface for capture. So much so that this development resulted in a 35% jump in US natural gas reserves from about 1,500 trillion ft^3 in 2006 to more than 2,000 trillion ft^3 in 2008 [84]. Note that this number is the total estimated reserves including speculative, possible, and probable sources, and of which only 237 trillion ft^3 is considered to be proven by the Energy Department. According to the same source, shale gas constitutes nearly a third of the total reserves.

Another potential source of natural gas is *gas hydrates* (also known as gas *clathrates*), which are "crystalline solids consisting of gas molecules, usually methane, each surrounded by a cage of water molecules." It looks very much like water ice. Methane hydrate is stable in ocean floor sediments at water depths greater than 300 m, and where it occurs, it is known to cement loose sediments in a surface layer several hundred meters thick. The worldwide amount of carbon bound in gas hydrates is conservatively estimated to total *twice the amount of carbon to be found in all known fossil fuels on Earth*. (Source: US Geological Survey Fact Sheet.)

Unfortunately, as of today, commercially feasible production of natural gas from gas hydrates is not a reality.

The dramatic increase in natural gas reserves and actual production via new technology that can extract it from shale rocks, taken at its face value, is a strong driver for its increasing share in electricity generation; at least in the USA. The advantage of natural gas vis-à-vis coal, which roughly accounts for half of US electricity generation, in terms of reduced carbon emissions is thus fortified from lower prices and increased availability. But the situation may not be as simple as it seems. The price of natural gas hit its 7-year low of about \$3/1,000 ft^3 in the summer of 2009. This huge drop from a peak of \$13 in the summer of 2008 was a direct result of the *great recession* that led to a decrease in demand, coupled with the increase in production. At the time of writing, NYMEX natural gas futures are trading at about \$4 per million Btu (about \$4.50/1,000 ft^3) and they were as high as \$6 per million Btu (about \$6.80/1,000 ft^3) at the beginning of 2010. Note that extremely low price levels are not likely to continue for long if they are below the production costs. Extreme price volatility can be expected when demand and supply (or capacity) go neck to neck.

In this context, one should also mention the problems associated with natural gas transportation via pipelines. In January 2009, the price quarrel between Russia and Ukraine ended in Russia cutting off all gas flows through Ukraine for 13 days. This resulted in severe distress in Southeastern Europe, which is nearly completely reliant on Russian gas, and other parts of Europe. While not an issue in North America, political stability of producer and transit countries is a significant concern for European countries that can make them reluctant in investing in natural gas–fired power plants. Alternate routes between Russia, Azerbaijan, and other countries, such as thousands of miles long *South Stream* and *Nabucco* pipelines, are actively pursued projects to provide answers to such concerns. The only other practical way to transport natural gas is to move it by sea by cooling it to $-162°C$ ($-260°F$) and converting it to a liquid (liquefied natural gas or LNG), which reduces its volume by 600 times. Specially built, double-hulled cryogenic ships are used to transport LNG from its port of origin to its port of destination, which are purpose-built facilities used exclusively to export or import LNG. From the receiving port, LNG is shipped to its final destination via tanker trucks, trains, or pipelines (after regasification). Expensive infrastructure investment requirements, safety concerns, large "carbon footprint" during liquefaction, transport, and regasification are key concerns associated with LNG, which limit its share in the overall natural gas consumption (currently less than 10% of US imports).

In terms of cost, regulatory costs, and incentives, e.g., those associated with GHG emission caps and cap-and-trade system requirements (e.g., for manufacturers and utilities to purchase pollution permits), should be considered along with straight dollars per Btu. Coal-fired generation can compete with natural gas in terms of GHG and other pollutant emissions only at a significantly high capital cost and reduced efficiency. Currently, there are two major approaches to accomplish this: Postcombustion carbon capture and storage (CCS) technologies that can clean the stack gas of the existing (via retrofit) and new coal-fired plants and precombustion

technologies that are a very good fit with *integrated gasification* CC (IGCC) power plants. Note that carbon emission abatement technologies via stack gas treatment are equally applicable to natural gas–fired CC power plants. In terms of both efficiency and cost, detailed studies indicate that NG-fired CC technology is superior to oil or coal-fired plants as well as IGCC [85].

Objectively viewed, these factors are strong incentives for natural gas burning power plants to replace aging, inefficient, and carbon-emitting, coal-fired power plants in the USA. To a certain extent, this can be accomplished even without building new natural gas-fired CC power plants. A recent report estimated that CC power plants had an average 2007 capacity factor of 42% [86]. In comparison, in the same year, coal-fired plants had a much higher capacity factor of 75%. Clearly, at least on paper, the replacement potential by simply switching generation from coal-fired to natural gas-fired plants is pretty big. In reality, factors such as geographical proximity of the power plants to each other and to the locations of highest demand, transmission system limitations and dispatch issues limited this potential severely; i.e., to about 5–9% of total US coal-based electricity generation [86]. While the proposed switch from coal to natural gas would also require an increase of 5–20% in natural gas supply, this should not be a significant problem in the light of recent developments discussed in the earlier paragraphs. A recent article states that several major US utilities have announced that they will replace at least some of their coal-fired plants slated for decommissioning (total capacity of more than 4.5 GW) [10].

Another factor that favors the natural gas–fired gas turbine plants over the coal-fired steam turbine power plants is operational flexibility. The rapid start-up and good turndown characteristics of gas turbine simple and combined cycle power plants, especially with the increase of renewable energy power plants (mostly solar and wind) connecting to the grid, make them eminently suitable to cyclic on-demand duties to compensate for the variability of the renewable generation. Presently, all major OEMs provide CC plants that can reach base load (several hundred megawatts) within 30–60 min without sacrificing base load efficiency, parts life, and RAM. Aeroderivative gas turbines, such as GE's intercooled LMS-100, can provide 100 MW within 10 min in an emergency or for peak shaving in hot summer months. Especially in Europe and to a certain extent in the USA, large, highly flexible natural gas–fired CC power plants that start and shut down daily for up to 250 starts and a total of 4,000 h of operation per year are expected to supplement renewable power generation. These plants are based on advanced F-Class and H-Class gas turbines that are rated at 58–59% efficiency and expected to reach more than 60% in the near future.

Clearly, then, no matter how regional politics in the USA, Europe, and other parts of the world play out, and what kind of legislative packages eventually emerge from governing bodies to control, cap or regulate carbon and other GHG emissions, natural gas–fired electricity generation with advanced gas turbine–based power plants will be an important part of the overall generating technology portfolio. In all likelihood, natural gas–fired advanced CC power plants will be the bridge technology between today's coal-based power generation and tomorrow's

renewable (and probably nuclear) power generation to alleviate the lurking problem of global warming. (In fact, this is pretty much the conclusion reached by a recent MIT report, which was made public after the writing of the present article [87].) The question is what will be the primary technologies in the next, say, quarter century?

Without a doubt, gas turbine–based power plants, in simple cycle (both heavy-duty industrial and aeroderivative variants) and combined cycle configurations will be by far the dominant technology in natural gas electric power generation. Today's advanced air-cooled F-Class and H-Class, steam-cooled G-Class, GE's H-System™, and J-Class engines with firing temperatures up to 1,600°C and PRs up to 23 (up to 35 in reheat machines) are currently capable of 58%, have recorded 59%, and are slated for 60% (or even 61% as claimed by one OEM) in 2011–2012 [88]. These are large units with 500–600 MW per block in 1×1 configuration designed not only for base load duty but for operational flexibility as described earlier. (In passing, note that the cited efficiencies are typically ISO rating numbers that reflect the most favorable operating assumptions (e.g., once-through open-loop cooling with water drawn from a natural source such as river, ocean, etc). Depending on site and ambient characteristics, performances of actual installed units will be somewhat lower with wide variability.)

Increasing power plant efficiency is the simplest and arguably the easiest way to reduce carbon emissions without breaking the bank or worrying about what to do with all that CO_2 or where to put it. As mentioned earlier, ambitious targets as high as 65% or even 70% have been in circulation for some time [57–60]. The discussion in the preceding sections of the article hopefully makes it clear that the key to ever-increasing gas turbine combined cycle efficiencies is increasing firing temperatures and commensurate cycle pressure ratios. The factors that prevent easy realization of that simple goal are primarily related to available component materials that can withstand the extreme pressures and temperatures and limits imposed by pollutant emission regulations. State-of-the-art nickel-based alloys used in turbine HGP components require significant amounts of cooling air supplied from extraction ports in the compressor, which is detrimental to performance. Higher flame zone temperatures in DLN combustors result in excessive NO_x and/or CO in flue gas, which is incompatible with increasingly stringent environmental regulations that limit the emissions of those pollutants to low single-digit numbers.

Single-crystal (SC) and directionally solidified (DS) superalloys with TBCs helped push firing temperatures up to 1,500°C. With closed-loop steam cooling and advanced film cooling techniques, J-Class turbines are rated at 1,600°C. Current research efforts focus on advances in materials, e.g., ceramic matrix composites (CMC) [58] or metal foams [59], which can reduce or even eliminate cooling air requirements at extremely high HGP temperatures. Manufacturing techniques have always been a significant driver in the implementation of aforementioned innovations; e.g., TBC application processes (e.g., electron beam physical vapor deposition), casting and machining technologies to produce SC airfoils. In a similar vein, laser-drilling and casting methods to achieve transpiration (effusion) cooling (the ultimate limit of film cooling) are related areas of research and development to further the goal of increasing turbine inlet temperatures. An

associated effort is made on the bottoming cycle side, i.e., development of HRSG heat exchanger tubes, steam headers and piping and steam turbine materials (casing, rotor, and buckets) that can withstand increased steam conditions as high as 180 bar and 600–700°C [89].

Closed-looped steam cooling of the combustor transition piece and stage-1 stators (nozzles) is an existing technique to increase the firing temperature without raising the combustor exit (turbine inlet) or flame temperatures [32, 33]. This enables performance improvement without a concomitant increase in NO_x emissions. Another method to facilitate extreme combustor exit and firing temperatures (up to 1,700°C) is exhaust gas recirculation (EGR), in which a fraction of the stack gas (up to 35%) is recirculated into the compressor or combustor inlet [90]. EGR reduces thermal NO_x production via reduced O_2 in combustion air and peak temperatures in flame. EGR's benefit becomes more pronounced at increased flame temperatures and it can reduce NO_x emissions by up to 50% [91]. EGR is also beneficial for postcombustion CCS because it increases the CO_2 concentration in stack gas (from ~3–4% to ~8–10% by volume), which leads to a reduction in the capital cost of the separation plant [91].

Lean premix or DLN combustion technology is the industry standard for heavy-duty industrial gas turbines for large-scale electricity production. In terms of the ability to meet the stringent emissions requirements, the technology is nearly at its limit at the current turbine inlet temperatures. EGR is one possibility to extend the applicability of DLN or even diffusion combustors to 1,700°C turbine inlet temperatures with low NO_x emissions. Another way to mitigate the NO_x emissions is selective catalytic reduction (SCR) in the HRSG. SCR is an existing postcombustion NO_x reduction technology. Other combustion technologies are being investigated for deployment in IGCC and other low-Btu syngas and blast-furnace gas applications to extend the fuel flexibility of gas turbines. The reader can consult the relevant sections in *The Gas Turbine Handbook* published by NETL (US DOE, Office of Fossil Energy). Various high-hydrogen and oxyfuel combustion technologies are being actively investigated for CO_2-free emissions. Since the subject of the present article is natural gas-burning technologies, the reader is referred to relevant academic journals such as *ASME's Journal of Engineering for Gas Turbines and Power*, which contain a wide selection of recent research papers on the subject.

A potentially promising combustion technology that directly attacks the single largest source of exergy destruction in the GT Brayton cycle is pulse detonation combustion (PDC). Originally proposed for jet engine aircraft propulsion, the technology has been around for more than a half century [92]. Recently, PDC is actively considered for land-based power generation [93]. The technology involves combustion of a fuel-air mixture across detonation waves in tubular devices [94]. Detonation waves are composite waves comprised of a "frozen" shock wave with pressure and temperature jump followed by a relaxation zone where chemical combustion reactions take place. The benefit of the process is temperature *and* pressure rise during the cycle heat addition process with a correspondingly higher mean-effective temperature vis-à-vis the conventional diffusion or DLN combustors with approximately constant

pressure (actually a 5–6% pressure loss). Detailed cycle calculations indicate that a PDC gas turbine in CC configuration is potentially 1.5–3 percentage points advantage over standard units at comparable firing temperatures and pressure ratios [95].

SOFC- or MCFC-based hybrid fuel cell plus gas turbine power plants are by far the most efficient future technologies to "burn" natural gas for electric power generation. In these machines, the fuel cell replaces the combustor to oxidize the gaseous fuel. Different configurations are possible. Detailed studies show that fuel cell-GT hybrid plants are capable of thermal efficiencies approaching 70%. Bhargava et al. [96] can be consulted for more information on these and other advanced GT-based power plants such as humid air turbine (HAT) and intercooled recuperated engine (ICR). Almost all variants have been studied in detail and reached various stages of development and commercialization in the past. They have not been able to pass the audition in terms of reliability, operability, capital cost, scalability, and other important considerations (e.g., water consumption) to present viable alternatives to simple Brayton cycle GT in CC configuration. Closed-loop steam cooling and reheat (also known as *sequential combustion*) have been the only successful and commercially accepted variations on the basic cycle. At this time, to the best of the authors' knowledge, there is no reason to expect this situation to change in the foreseeable future; at least in terms of large-scale electric power generation. As always, dual-fuel diesel engines capable of burning gaseous fuels will continue to play a role in small-scale and/or distributed generation applications. The same can be true for very small (several kilowatts) fuel cell–based hybrid units.

Bibliography

Primary Literature

1. Energy Information Administration (EIA) (2009) Annual energy review 2008. http://www.eia.doe.gov/aer. Accessed 29 June 2009
2. Energy Information Administration (EIA) (2008) International energy outlook 2008. DOE/EIA-0484(2008). www.eia.doe.gov/oiaf/ieo/index.html.
3. United States Environmental Protection Agency (EPA) (2010) Methane. www.epa.gov/methane.
4. Liss WH, Thrasher WR (1992) Variability of natural gas composition in select major metropolitan areas of the United States. Gas Technology Institute, Chicago, GRI-92/013
5. Natural Gas and the Environment (2010) From http://www.naturalgas.org/environment/naturalgas.asp
6. Turbomachinery International (2008) 49(6), 10/2008, Handbook 2009. www.turbomachinerymag.com
7. Wärtsilä 50DF generating set (2010) From www.wartsila.com
8. Khan BH (2006) Non-conventional energy sources. Tata McGraw Hill, New Delhi, India
9. McNeely M (2006) Power generation order survey. Diesel & Gas Turbine Worldwide. Article from Oct 2006 issue

10. Burt B, Mullins S (2010) U.S. gas-fired power development: last man standing, POWER. http://www.powermag.com. Accessed Sept 2010, pp 71–73
11. Wilson DG, Korakianitis T (1998) The design of high efficiency turbomachinery and gas turbines, 2nd edn. Prentice-Hall, Uppersaddle River
12. Von Ohain H (1996) Foreword. In: Mattingly JD (ed) Elements of gas turbine propulsion. Tata McGraw Hill, New Delhi, India, Edition 2005
13. Meher-Homji CB (1997) The development of the Junkers Jumo 004B – the world's first production turbojet. J Eng Gas Turb Power 119:783
14. Meher-Homji CB (1998) The development of the Whittle Turbojet. J Eng Gas Turb Power 120:249
15. Meher-Homji CB (2000) Pioneering turbojet developments of Dr. Hans von Ohain – from the HeS 1 to the HES 011. J Eng Gas Turb Power 122:191
16. Soares C (2006) Gas turbines in simple cycle and combined cycle applications. Section 1.1 in The gas turbine handbook. US DOE, Office of Fossil Energy, NETL. http://www.netl.doe.gov/technologies/coalpower/turbines/refshelf/handbook/TableofContents.html
17. Leiste V (1999) Development of the siemens gas turbine and technology highlights. Siemens Power Generation, Erlangen, Germany
18. Miller H, Nemec T (2006) Gas turbines. In: Myer K (ed) Mechanical engineers' handbook, 3rd edn., Energy and power. Wiley, Hoboken, Chapter 24
19. Brandt D (2007) A brief history of GE energy product lines. General Electric Company, New York
20. Brandt D (1988) The design and development of an advanced heavy-duty gas turbine. J Eng Gas Turb Power 110:243–250
21. Stodola A (1927) Steam & gas turbines. Authorized translation from the 6th German edition: Löwenstein LC. McGraw-Hill, New York
22. Langston LS (2010) World's first gas turbine power plant. ASME Mech Eng 132(4):51
23. Tomlinson LO, Lee DT (1985) Combined cycles. In: Sawyer JW, Japikse D (eds) Sawyer's gas turbine engineering handbook, Chapter 7. Turbomachinery International Publications, Norwalk, Conn., USA
24. Horlock JH (1994) Combined cycle power plants – past, present, and future. J Eng Gas Turb Power 117:608–616
25. Gebhardt E (2000) The F Technology experience story, GER-3950C. http://www.gepower.com/
26. Haselbacher H (1989) Gas turbine fundamentals. In: Elliott TC (ed) Standard handbook of power plant engineering. New York, McGraw-Hill Publishing POWER magazine
27. Horlock JH (1997) Aero-engine derivative gas turbines for power generation: thermodynamic and economic perspectives. J Eng Gas Turb Power 119:119–123
28. Moran MJ, Shapiro HN (1988) Fundamentals of engineering thermodynamics. Wiley, New York
29. Cohen H, Rogers GFC, Saravanamuttoo HIH (1987) Gas turbine theory, 3rd edn. Longman, London
30. Cumpsty N (2003) Jet propulsion, 2nd edn. Cambridge University Press, Cambridge
31. Schilke PW (2004) Advanced gas turbine materials and coatings, GER-3569 G. www.gepower.com
32. Pritchard JE (2003) H-System™ technology update. GT2003-38711, ASME turbo expo – power for land, sea & air, 16–19 June 2003, Atlanta
33. Koeneke C (2006) Steam cooling of large frame gas turbines one decade in operation. VDI Ber Nr 1965:33–42
34. Imwinkelried B (1995) Advanced cycle system gas turbines GT24/GT26: the highly efficient gas turbines for power generation. In: Proceedings of the 21st international congress on combustion engines, CIMAC 1995, Interlaken, Switzerland
35. Chiesa P, Macchi E (2004) A thermodynamic analysis of different options to break 60% electric efficiency in CC power plants. J Eng Gas Turb Power 126:770–785

36. Holland MJ, Thake TF (1980) Rotor blade cooling in high pressure turbines. J Aircr 17:412–418
37. Elmasri MA, Pourkey F (1986) Prediction of cooling flow requirements for advanced utility gas turbines. Part 1: analysis and scaling of the effectiveness curve, 86-WA/HT-43, ASME Winter Annual Meeting, Anaheim, 7–12 Dec 1986
38. Elmasri MA (1986) Prediction of cooling flow requirements for advanced utility gas turbines. Part 2: influence of ceramic thermal barrier coatings. ASME Winter Annual Meeting, Anaheim, 7–12 Dec 1986
39. Elmasri MA (1985) On thermodynamics of gas turbine cycles: part 1 – second law analysis of combined cycles. J Eng Gas Turb Power 107:880–889
40. Elmasri MA (1986) On thermodynamics of gas turbine cycles: part 2 – a model for expansion in cooled turbines. J Eng Gas Turb Power 108:151–159
41. Elmasri MA (1986) On thermodynamics of gas turbine cycles: part 3 – thermodynamic potential and limitations of cooled reheat gas turbine combined cycles. J Eng Gas Turb Power 108:160–170
42. Horlock JH, Watson DT, Jones TV (2001) Limitations on gas turbine performance imposed by large turbine cooling flows. J Eng Gas Turb Power 123:487–494
43. Horlock JH (2001) The basic thermodynamics of turbine cooling. J Eng Gas Turb Power 123:583–591
44. Wilcock RC, Young JB, Horlock JH (2005) The effect of turbine blade cooling on the cycle efficiency of gas turbine power cycles. J Eng Gas Turb Power 127:109–120
45. Young JB, Wilcock RC (2002) Modeling the air-cooled gas turbine: parts 1 and 2. J Turbomach 124:207–222
46. Gülen SC (2010) A simple mathematical model for cooled gas turbines. GT2010-22160, ASME turbo expo – power for land, sea & air, 14–18 June 2010, Glasgow
47. Rice IG (1995) Steam-injected gas turbine analysis: steam rates. J Eng Gas Turb Power 117:347–353
48. Cheng DY, Nelson ALC (2002) The chronological development of the Cheng cycle steam injected gas turbine during the past 25 years. ASME International – IGTI Turbo Expo 2002, GT2002-30119
49. Rao A (1989) Process for producing power. U.S. Patent No. 4,289,763
50. Adelman ST, Hoffman MA, Baughn JW (1995) A methane-steam reformer for a basic chemically recuperated gas turbine. J Eng Gas Turb Power 117:16–23
51. McDonald CF, Boland CR (1981) The Nuclear Closed-Cycle Gas Turbine (HTGR-GT) – dry cooled commercial power plant studies. J Eng Gas Turb Power 103:89–100
52. Reale MJ (2004) New high efficiency simple cycle gas turbine – GE's LMS100™, GER-4222A. www.gepower.com
53. Mercury 50, Recuperated Gas Turbine Generator Set, Solar® Turbines (2010) www.solarturbines.com
54. Cox JC, Hutchinson D, Oswald JI (1995) The Westinghouse/Rolls Royce WR-21 gas turbine variable area power turbine design. ASME Paper 95-GT-54, International Gas Turbine and Aeroengine Congress and Exposition, Houston, TX, 5–8 June 1995
55. Hofer DC, Gülen SC (2006) Efficiency entitlement for bottoming cycles. GT2006-91213, ASME turbo expo – power for land, sea & air, Barcelona, Spain, 8–11 May 2006
56. Gülen SC, Smith RW (2008) Second law efficiency of the Rankine bottoming cycle of a combined cycle power plant. ASME Paper GT2008-51381. ASME turbo expo 2008, Berlin, Germany, 9–13 June 2008
57. Bohn D (2006) SFB 561: Aiming for 65% CC efficiency with an air-cooled GT, Modern Power Systems, pp 26–29, Sept 2006
58. Mutassim Z (2008) New gas turbine materials. Turbomachinery International, Sept/Oct 2008 issue, 38–42
59. Bohn D, Dilthey U, Schubert F (2004) Innovative Technologien für ein GuD-Kraftwerk mit 65% Wirkungsgrad. VDI-Berichte Nr 1857:13–25

60. Rao AD, Robson FL, Geisbrecht RA (2002) Power plant system configurations for the 21st century. In: ASME turbo expo 2002, Amsterdam, the Netherlands, 3–7 June 2002
61. Lundberg WL, Veyo SE, Moeckel MD (2003) A high efficiency solid oxide fuel cell hybrid power system using the mercury 50 advanced turbine system gas turbine. ASME J Eng Gas Turb Power 125:51–58
62. Massardo AF, Lubelli F (2000) Internal Reforming Solid Oxide Fuel Cell – Gas Turbine Combine Cycles (IRSOFC-GT); Part I: cell model and cycle thermodynamic analysis. ASME J Eng Gas Turb Power 122:27–35
63. Massardo AF, Magistri L (2003) Internal Reforming Solid Oxide Fuel Cell – Gas Turbine Combine Cycles (IRSOFC-GT); Part II: exergy and thermoeconomic analyses. ASME J Eng Gas Turb Power 125:67–74
64. Chase DL, Kehoe PT. GE combined-cycle product line and performance, GER-3574 g. GE Energy
65. Chris EM, Leroy OT. GE combined-cycle experience, GER-3651. http://www.gepower.com.
66. Tomlinson LO, McCullough S. Single-shaft combined – cycle power generation system, GER-3767c. http://www.gepower.com
67. Matta RK, Mercer GD, Tuthill RS. Power systems for the 21st century – H GT combined-cycles, GER-3935B. GE Energy
68. Smith RW, Polukort P, Maslak CE, Jones CM, Gardiner BD. Advanced technology combined cycles, GER-3936a. GE Power Systems
69. Phylipsen GJM, Blok K, Worrell E (1998) Handbook on international comparisons of energy efficiency in the manufacturing industry. Department of Science, Technology and Society, Utrecht University, The Netherlands
70. Gülen SC (2010) A proposed definition of CHP efficiency, POWER. http://www.powermag.com, pp 58–63, June 2010
71. European Association for the Promotion of Cogeneration (Mar 2001) A guide to cogeneration. http://www.cogeneurope.eu/wp-content/uploads//2009/02/educogen_cogen_guide.pdf
72. Energy Information Administration (EIA) (2009) Annual energy review 2008. http://www.eia.doe.gov/aer. Accessed 29 June 2009
73. Energy Information Administration (EIA) (2010) Electric power annual. http://www.eia.doe.gov/fuelelectric.html. Accessed 20 Jan 2010
74. Davis LB, Black SH (2000) Dry low nox combustion systems for GE heavy-duty gas turbines, GER-3568 g. http://www.gepower.com
75. Lefebvre AH (1995) The role of fuel preparation in low-emission combustion. J Eng Gas Turb Power 117:617
76. Roointon, Pavri, Moore, Gerald D (2001) Gas turbine emissions and control, GER-4211. http://www.gepower.com
77. Hilt MB, Waslo J (October 1984) Evolution of NOx abatement techniques through combustor design for heavy-duty gas turbines. J Eng Gas Turb Power 106:825
78. Touchton GL (1984) An experimentally verified NOx prediction algorithm incorporating the effects of steam injection. J Eng Gas Turb Power 106:833
79. Davi MA (1994) GE gas turbine combustion flexibility, GER-3946. GE Energy
80. Miller HE (1994) Development of the GE quiet combustor and other design changes to benefit quality, GER-3551. http://www.gepower.com
81. Peters M, Timmerhaus K, West R (2004) Plant design and economics for chemical engineers, 5th edn. McGraw-Hill, London
82. Bejan A, Tsatsaronis G, Moran M (1996) Thermal design & optimization. Wiley, New York
83. Kehlhofer R, Warner J, Nielsen H, Bachmann R (1999) Combined cycle gas & steam turbine power plants, 2nd edn. PennWell Corp, Tulsa
84. As reported in the press per Potential Gas Committee report (2008) Potential supply of natural gas in the United States, Potential Gas Agency, Colorado School of Mines, Golden, 31 Dec 2008

85. Gambini M, Vellini M (Jan 2003) CO_2 emission abatement from fossil fuel power plants by exhaust gas treatment. J Eng Gas Turb Power 125:365–373
86. Wagman D (2010) Can natural gas displace coal? Power Eng (Mar 2010 issue): 4
87. The future of natural gas – an interdisciplinary MIT study (2010) Interim report by MIT Energy Initiative, ISBN 978-0-9828008-0-5, Massachusetts Institute of Technology, Boston
88. Robb D (2010) CCGT: breaking the 60 percent efficiency barrier. Power Eng Int 18(3). www.peimagazine.com
89. Review of status of advanced materials for power generation, Technology Status Report, Cleaner Coal Technology Programme, Department of Trade and Industry (Oct 2002) London
90. Tukagoshi K, Muyama A, Uchida S et al (Oct 2005) Latest technology for large capacity gas turbine. MHI Tech Rev 42(3)
91. ElKady AM, Evulet A, Brand A (May 2009) Application of exhaust gas recirculation in a DLN F-class combustion system for postcombustion carbon capture. J Eng Gas Turb Power 131: #034505
92. Kailasanath K (2000) Review of propulsion applications of detonation waves. AIAA J 38(9):1698–1708
93. Goldmeer J, Tangirala V, Dean A (2008) System-level performance estimation of a pulse detonation based hybrid engine. J Eng Gas Turb Power 130:#011201
94. Tangirala VE, Rasheed A, Dean AJ (2007) Performance of a pulse detonation combustor-based hybrid engine, GT2007-28056. ASME turbo expo – power for land, sea & air, Montreal, Canada, 14–18 June 2007
95. Gülen SC (2010) Gas turbine with constant volume heat addition. ESDA2010-24817. ASME 2010 10th biennial conference on engineering systems design and analysis, Istanbul, Turkey, 12–14 July 2010
96. Bhargava R, Bianchi M, Campanari S et al (2010) A parametric thermodynamic evaluation of high performance gas turbine based power cycles. J Eng Gas Turb Power 132:#022001

Books and Reviews

Bejan A (2006) Advanced engineering thermodynamics, 3rd edn. Wiley, New Jersey
Boss M (1996) Steam turbines for STAG™ combined cycle power systems, GER-3582E. http://www.gepower.com
Boyce MP (2006) Gas turbine engineering handbook, 3rd edn. Gulf Professional Publishing, Houston
Chase D (2001) Combined cycle development evolution and future, GER-4206. http://www.gepower.com
Colegrove D, Mason P, Retzlaff K, Cornell D (2001) Structured steam turbines for the combined cycle market, GER-4201. http://www.gepower.com
Constant EW II (1980) The origins of the turbojet revolution. The Johns Hopkins University Press, Baltimore/London
Cotton KC (1998) Evaluating and improving steam turbine performance, 2nd edn. Cotton Fact Inc, Rexford
Denton JD (1993) Loss mechanisms in turbomachines, The 1993 IGTI scolar lecture. J Turbomachinery 115:621–656
Dunn MG (2001) Convective heat transfer and aerodynamics in axial flow turbines. J Eng Gas Turb Power 123:637–686
Elmasri MA (2007) Design of gas turbine combined cycle and cogeneration systems – theory, practice and optimization. Seminar Notes, Thermoflow, Inc., Sudbury, MA. info@thermoflow.com

Han JC, Dutta S, Ekkad SV (2000) Gas turbine heat transfer and cooling technology. Taylor & Francis, New York
Horlock JH (2001) Combined power plants: including Combined Cycle Gas Turbine (CCGT) Plants. Krieger Publishing Company, Malabar
Kehlhofer R, Hannemann F, Stirnimann F, Rukes B (2009) Combined cycle gas & steam turbine power plants, 3rd edn. PennWell Corp, Tulsa
Lakshminarayana B (1996) Fluid dynamics and heat transfer of turbomachinery. Wiley, New York
Lefebvre AH, Ballal DR (2010) Gas turbine combustion: alternative fuels and emissions, 3rd edn. CRC Press/Taylor & Francis, Boca Raton
Nag PK (2006) Power plant engineering, 2nd edn. Tata McGraw-Hill, New Delhi, India
Saravanamuttoo HIH, Rogers GFC, Cohen H, Straznicky PV (2009) Gas turbine theory, 6th edn. Pearson Prentice Hall, England
Traupel W (1977) Thermische Turbomaschinen, Erster Band, Thermodynamisch-strömungstechnische Berechnung, 3, neuarbeitete und erweiterte Auflage. Springer, Berlin/Heidelberg/New York